Geochemistry, Geophysics, Geosystems®

AGU ADVANCING EARTH AND SPACE SCIENCE

RESEARCH ARTICLE
10.1029/2021GC010013

Melting and Evolution of Amphibole-Rich Back-Arc Abyssal Peridotites at the Mado Megamullion, Shikoku Basin

A. Sen[1,2], J. E. Snow[2], Y. Ohara[3,4,6], K. Hirauchi[5], Y. Kouketsu[6], A. Sanfilippo[7], V. Basch[7], Y. Harigane[8], M. Fujii[9], K. Okino[10], and N. Akizawa[10]

[1]Department of Earth and Atmospheric Sciences, University of Houston, Houston, TX, USA, [2]Department of Geology and Geophysics, Louisiana State University, Baton Rouge, LA, USA, [3]Hydrographic and Oceanographic Department of Japan, Tokyo, Japan, [4]Research Institute for Marine Geodynamics, Japan Agency for Marine-Earth Science and Technology (JAMSTEC), Yokosuka, Japan, [5]Department of Geosciences, Faculty of Science, Shizuoka University, Shizuoka, Japan, [6]Graduate School of Environmental Studies, Nagoya University, Nagoya, Japan, [7]Dipartimento di Scienze della Terra e dell'Ambiente, University of Pavia, Pavia, Italy, [8]Research Institute of Geology and Geoinformation, Geological Survey of Japan, National Institute of Advanced Industrial Science and Technology (AIST), Tsukuba, Japan, [9]National Institute of Polar Research/SOKENDAI, Tokyo, Japan, [10]Atmosphere and Ocean Research Institute, The University of Tokyo, Chiba, Japan

Key Points:

- Partial melting and melt-rock reaction in back-arc basin peridotites
- Presence of pargasitic amphiboles in the peridotites and crystallization in a hydrous environment
- Influx of enriched melts which reproduces the enriched signatures in the Shikoku Basin basalts

Supporting Information:

Supporting Information may be found in the online version of this article.

Correspondence to:

A. Sen,
atlantasen@gmail.com

Citation:

Sen, A., Snow, J. E., Ohara, Y., Hirauchi, K., Kouketsu, Y., Sanfilippo, A., et al. (2021). Melting and evolution of amphibole-rich back-arc abyssal peridotites at the Mado Megamullion, Shikoku Basin. *Geochemistry, Geophysics, Geosystems*, *22*, e2021GC010013. https://doi.org/10.1029/2021GC010013

Received 6 JUL 2021
Accepted 15 NOV 2021

Abstract The Mado Megamullion is an oceanic core complex (OCC) in the Shikoku back-arc basin within the Philippine Sea Plate. Mantle peridotites (serpentinized) recovered by six dredge and submersible cruises exhibit signatures of extensive deformation. Amorphous pseudomorphs after plagioclase in many of the samples, as well as plagioclase-spinel intergrowths, are clear evidence of melt stagnation and mantle reaction. Spinels show a wide range of compositions in terms of their Cr#, Mg#, and TiO_2 content. The presence of apparently magmatic high-temperature pargasitic amphibole in veins and as replacement of clinopyroxene suggests that it may be a primary or near-primary mineral crystallized from a hydrous melt which is unusual for abyssal peridotites. Two trace-element populations of clinopyroxenes are in equilibrium with depleted and enriched basaltic melts, respectively. Rare-earth element (REE) in the most depleted clinopyroxenes are modeled by 10% fractional melting except for a ubiquitous La-Ce "kick." Multiple models of open system melting combined with subsequent mixing of an enriched melt can explain the REE data. Broadly it appears that the peridotites underwent variable degrees of partial melting with moderate influx of enriched melts, which agrees with the other textural and chemical evidence of melt-rock reaction and re-fertilization. The compositions of the accumulated melts simulated by the open system models reproduce the enrichments in fluid mobile elements (Ba, U, and Pb) observed in basalts dredged from the Shikoku basin. Back-arc basin peridotites at Mado Megamullion appear to have a unique petrographic and geochemical character that is distinct from those of peridotites exposed at the seafloor after formation from mid-ocean ridges.

1. Introduction

Oceanic core complexes (OCCs) are characterized by the presence of domal bathymetric highs with spreading-axis-normal striations (Cann et al., 1997; Escartín & Canales, 2011; Tucholke et al., 1998). These structures were first identified at the Mid-Atlantic Ridge (Blackman et al., 1998; Cann et al., 1997; Karson, 1990; Tucholke et al., 1998). They are interpreted to be formed by the exhumation of the lithosphere along low-angle detachment faults at slow spreading rates ranging between 14 to 75 mm/year (Blackman et al., 2009). Gabbros and peridotites from the young lithosphere are exposed at the seafloor (Tucholke et al., 2008). These provide useful insights into the processes of crustal accretion, the architecture of the oceanic lithosphere and the mantle dynamics, which connects magmatism to tectonics at mid-oceanic ridges (Escartín et al., 2003; Macleod et al., 2002). Peridotites exposed along detachment faults (Dick et al., 2010; Escartín et al., 2003; Warren & Shimizu, 2010) are characterized by the presence of deformation fabrics and alteration features (Harigane et al., 2011a; Loocke et al., 2013; Macleod et al., 2002; Ohara, 2016). The detachment faulting is therefore thought to have initiated in the lower crust (melt-rich zone) and ceased during or prior to its exhumation (Blackman et al., 2005, 2009; Dick et al., 1991, 2000). Prior studies on OCCs have mostly been conducted along slow-spreading Mid-Atlantic Ridge (Blackman et al., 2006; Dick et al., 2008; Escartín et al., 2008; Kelemen et al., 2004; Macleod et al., 2009; Parnell-Turner et al., 2018; Sdrolias et al., 2004; Smith et al., 2008) and ultraslow-spreading Southwest Indian Ridge (Dick et al., 2002; Dick, Kvassnes, et al., 2019; Dick, MacLeod, et al., 2019; Baines et al., 2003; Sauter et al., 2013). Other than mid-oceanic ridge settings, the Godzilla Megamullion (Ohara et al., 2001) in the Parece

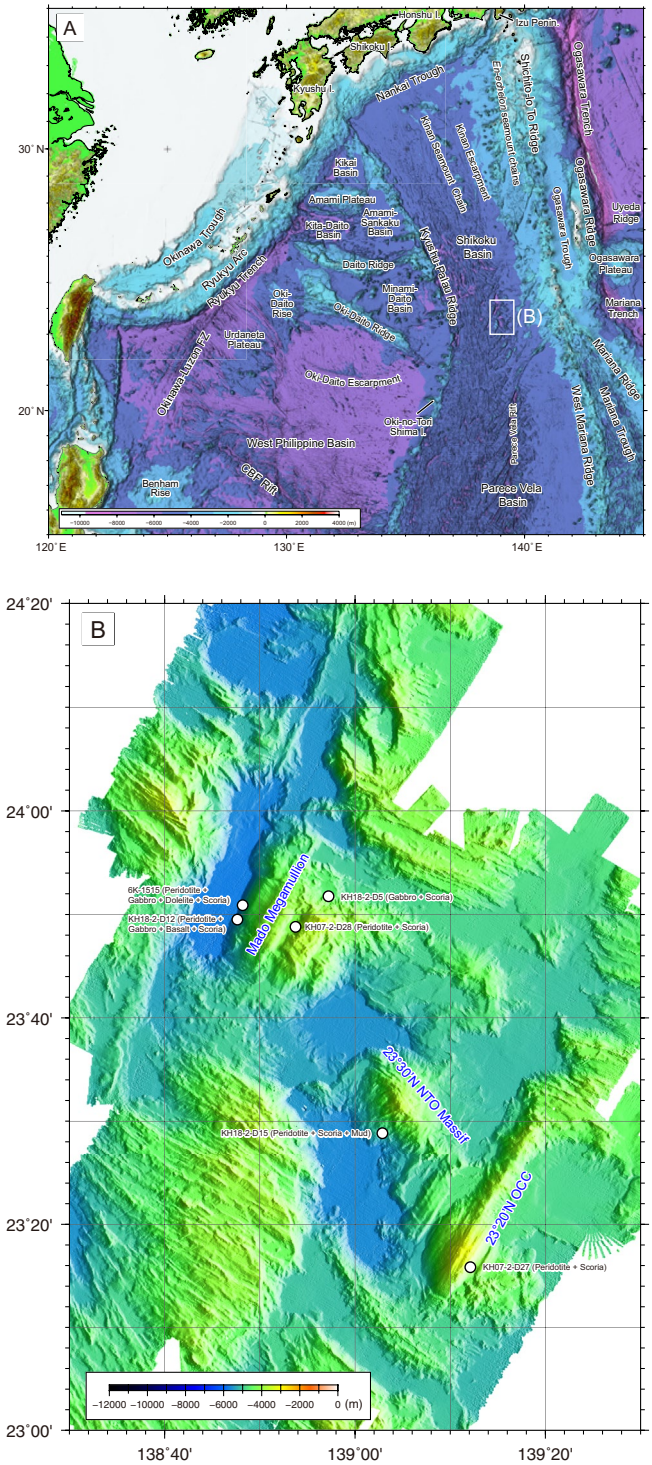

Figure 1. (a) Bathymetric map of Philippine Sea plate comprising different tectonic elements after Taira et al. (2016). The white square indicates the Mado Megamullion area. (b) Dredge and dive site locations in a detailed map of the Mado Megamullion area where most of the peridotite samples were recovered from the transform wall.

Vela Basin in the Philippine Sea remains the only OCC that has been extensively studied in a back-arc spreading environment until present (Harigane et al., 2008, 2011a, 2011b; Loocke et al., 2013; Michibayashi et al., 2014; Ohara et al., 2003, 2007; Okino et al., 1999; Sanfilippo et al., 2013; Spencer & Ohara, 2014; Tani et al., 2011). The study of OCCs in back-arc spreading environments helps understand mantle architecture, magmatic and tectonic evolution of global OCCs, and the evolutionary dynamics and processes that operate in back-arc environments.

In this study, we introduce and present data from mantle peridotites that were sampled from the Mado Megamullion, a recently discovered OCC in the back-arc spreading environment of the Shikoku Basin in the Philippine Sea (Akizawa et al., 2021; Basch et al., 2020; Hirauchi et al., 2021; Ohara et al., 2018; Okino et al., 2019). This study focuses on the petrography and geochemical evolution of the peridotites in terms of the degree of partial melting, melt-rock reaction, and the role of water during its exhumation.

2. Geological Setting

The Philippine Sea Plate is a large and complex tectonic plate made of active and extinct back-arc basins, and arcs and remnant arcs in the Western Pacific region. The Parece Vela Basin, Shikoku Basin and West Philippine Basin are extinct back-arc basins whereas the Mariana Trough is an active back-arc basin (Karig, 1975; Kasuga & Ohara, 1997; Okino et al., 1999). The Parece Vela and Shikoku back-arc basins are inter-connected at ~25°N (Okino et al., 1999). They are located between the Kyushu-Palau Ridge to the west and West Mariana Ridge and the Izu-Bonin Arc to the east (Okino et al., 1999) (Figure 1a). The two basins have a common evolutionary history. Magnetic anomaly data have revealed that both basins opened as a single back-arc system. Subsequently, after 19 Ma, there was a shift in the spreading direction and the extinct axes of the two basins show a different spreading orientation (Okino et al., 1999). The Shikoku Basin formed in two stages initiated by the subduction of the western margin of the Pacific Plate. In contrast to the Parece Vela Basin, spreading in the Shikoku Basin started in the northern end and propagated southward. The spreading direction changed from ENE-WSW to NE-SW. The axial zone is dominated by post-spreading volcanism known as the Kinan Seamount Chain in the Shikoku Basin while the Parece Vela Basin has a set of low-lying depressions also known as the Parece Vela Rift (Ohara et al., 2001; Okino et al., 1999).

Geological and geophysical data collected by Japan's Continental Shelf Survey have revealed the presence of oceanic core complexes in the Philippine Sea Plate (Ohara et al., 2015). The Godzilla Megamullion in the Parece Vela Basin (Harigane et al., 2008, 2011a, 2011b; Loocke et al., 2013; Michibayashi et al., 2014; Ohara, 2016; Ohara et al., 2001, 2003; Okino et al., 1999; Sanfilippo et al., 2013; Spencer & Ohara, 2014; Tani et al., 2011) has a corrugated morphology, which is typical of OCCs found along other slow-spreading ridges (Blackman et al., 1998; Cann et al., 1997; Cannat et al., 1995; Dick et al., 2003; Tucholke et al., 1998), and is the largest known OCC on Earth (Ohara, 2016). It is divided into proximal, medial, and distal regions and its development has been interpreted to be formed by melt-rock interaction resulting in detachment fault nucleation and weakening that may have exhumed large volumes of mantle rocks (Loocke et al., 2013). To date, it is the only well-studied OCC in a back-arc environment.

The Mado Megamullion was first sampled by KH07-2 cruise in 2007 and further investigated by recent KH18-2, YK18-07, and YK19-04S cruises (Basch et al., 2020; Ohara et al., 2019). Multibeam bathymetry and gravity studies revealed the presence of spreading-parallel corrugations and high mantle Bouguer gravity anomaly (~20 mGal higher than the surroundings) in the Mado Megamullion and the Non-Transform Offset (NTO) massif (Ohara et al., 2018, 2019; Okino et al., 2019) (Figure 1b). These geophysical observations are coupled with the presence of gabbros and peridotites sampled from the Mado Megamullion by dredges and Shinkai 6500 dives (Basch et al., 2020; Ohara et al., 2019) (Figure 1b). The total area of the Mado Megamullion is ~550 km^2, which is much smaller in size than the Godzilla Megamullion (~7,200 km^2) but can be compared to other typical OCCs like the Kane Megamullion in the Mid-Atlantic Ridge (Dick et al., 2008; Karson & Dick, 1983).

The cruise KH07-02 in 2007 recovered small amounts of serpentinized peridotite. This was followed by the KH18-2 dredging cruise and Shinkai 6500 diving expeditions YK18-07 in 2018 and YK19-04S in 2019 that extensively mapped and collected samples from the area. These cruises recovered a wide range of samples that include serpentinized peridotites, gabbros, dolerite intrusions, pillow basalts and sediments. In this study, we have focused on the peridotites that were sampled by cruises KH07-02, YK18-07, and KH18-2.

3. Samples

We have studied a total of 26 peridotite samples: 19 that were collected by the R/V Hakuho Maru KH18-2 dredging cruise in 2018. Dredge sites D12 and D15 recovered peridotites. The only peridotite recovered from D15 was highly altered and could only be used for elemental analysis of silicates. Our set of samples also includes six peridotites that were collected by R/V Yokosuka YK18-07 cruise using the DSV Shinkai 6500 submersible (at Dive 6K1515) and one peridotite recovered by the R/V Hakuho Maru KH07-02 dredging cruise in 2007 at dredge site D28 (Table 1).

3.1. Petrographic Analysis

The peridotites are mostly serpentinized (Hirauchi et al., 2021) lherzolites and dunites containing clinopyroxene, orthopyroxene, serpentinized olivine, spinel and altered plagioclase (Figure 2). The modal proportion of clinopyroxenes in the lherzolites (fertile to depleted) varies from about 1% to 15%. Some of the lherzolites are highly altered where pyroxenes are replaced by secondary hydrous minerals although they preserve their primary morphology. The dunite samples contains olivine that has been completely serpentinized, spinel is the only primary mantle mineral that could be studied (Figure 2c). Spinels are present either as holly leaf morphology typical of mantle spinels (Figure 3a) or as worm-like intergrowths (Figure 3b). Altered plagioclase is present (as pseudomorphous material) as replacement coronas around spinels or clinopyroxenes but also as symplectite intergrowth with worm-like spinels (Figures 3b and 3c). As plagioclase is generally considered a characteristic related to melt stagnation, we classified the peridotites petrographically as (a) plagioclase absent and (b) plagioclase present (Figures 3a–3c).

Some of the lherzolites have been crosscut by different late-stage veins. Sulfide mineralization is observed in some of the veins of KH18-2-D12 samples (Figure 2d). The samples show signatures of deformation in the form of porphyroclastic textures and mylonitized fabrics (Figure 3d). Amphiboles are present in nearly all the samples as (a) a replacement phase over pyroxenes or (b) within leucocratic veins. Late-stage amphibole-chlorite-Ti-oxide bearing leucocratic veins with traces of zircons and apatites are present in samples from both KH18-2 and YK18-07 cruises (Figure 2e). These samples are classified as peridotites with veins.

3.2. Clinopyroxene-Orthopyroxene Exsolution and Spinel Exsolution in Clinopyroxene

The primary mantle minerals from KH18-2 display extensive exsolution. Exsolution lamellae of clinopyroxene are present in orthopyroxene. These exsolution lamellae warp along the deformation or shear planes (Figure 3e). The clinopyroxenes contain exsolution lamellae of chromium-rich oxides (probably chrome spinels) (Figure 3f). This indicates that the pyroxenes re-equilibrated at lower temperatures and pressures.

Table 1
Location and Lithology of Peridotites From the Mado Megamullion

Cruise	Sample no	Latitude(N)	Longitude(E)	Water depth(m)	Lithology	Comment
KH18-2	D12-R34	23°49.306′	138°47.635′	5,403	Dunite (serpentinized olivine)	Plg present
KH18-2	D12-R17	23°49.306′	138°47.635′	5,403	Lherzolite (deformed)	Amp present
KH18-2	D12-R02	23°49.306′	138°47.635′	5,403	Lherzolite (altered)	Plg present
KH18-2	D12-R12	23°49.306′	138°47.635′	5,403	Serpentinized	
KH18-2	D12-R20	23°49.306′	138°47.635′	5,403	Lherzolite	Plg present; Amp present
KH18-2	D12-R06	23°49.306′	138°47.635′	5,403	Lherzolite	Plg present; Amp present
KH18-2	D12-R19	23°49.306′	138°47.635′	5,403	Lherzolite	Amp present
KH18-2	D12-R08	23°49.306′	138°47.635′	5,403	Lherzolite (deformed)	Amp present
KH18-2	D12-R04	23°49.306′	138°47.635′	5,403	Lherzolite (altered)	Amp present
KH18-2	D12-R11	23°49.306′	138°47.635′	5,403	Lherzolite (altered)	Amp present
KH18-2	D12-R18	23°49.306′	138°47.635′	5,403	Lherzolite (deformed)	Amp present
KH18-2	D12-R14	23°49.306′	138°47.635′	5,403	Lherzolite	
KH18-2	D12-R01	23°49.306′	138°47.635′	5,403	Lherzolite	Plg present; Amp present
KH18-2	D12-R10	23°49.306′	138°47.635′	5,403	Lherzolite (deformed)	Amp present
KH18-2	D12-R07	23°49.306′	138°47.635′	5,403	Lherzolite (altered)	Plg present
KH18-2	D12-R33	23°49.306′	138°47.635′	5,403	Lherzolite (deformed)	Amp present
KH18-2	D12-R05	23°49.306′	138°47.635′	5,403	Lherzolite	Plg present; Amp present
KH18-2	D12-R15	23°49.306′	138°47.635′	5,403	Lherzolite	Plg present; Amp present
KH18-2	D12-R03	23°49.306′	138°47.635′	5,403	Lherzolite (altered)	Plg present;
YK18-07	6K-1515-R10	23°50.500′	138°48.257′	5,295	Lherzolite	Peridotite with vein; Amp present
YK18-07	6K-1515-R09	23°50.500′	138°48.257′	5,295	Lherzolite	Peridotite with vein; Amp present
YK18-07	6K-1515-R03	23°50.600′	138°48.089′	5,680	Lherzolite (deformed)	Amp present
YK18-07	6K-1515-R15	23°50.400′	138°48.437′	5,025	Lherzolite	Amp present
YK18-07	6K-1515-R02	23°50.600′	138°47.923′	5,673	Lherzolite	Amp present
YK18-07	6K-1515-R06	23°50.600′	138°48.089′	5,483	Lherzolite (altered)	Peridotite with vein; Amp present
KH07-02	D28-001	23°48.266′	138°53.544′	4,074	Lherzolite	

Note. Classification is based on the petrography and chemistry of spinels (see text).

4. Analytical Methods

4.1. Major Element Analysis

We analyzed the major element concentration of silicates and spinel at Rice University by using a JEOL JXA 8530F Hyperprobe with a field emission assisted thermo-ionic (Schottky) emitter, equipped with five Wavelength Dispersive Spectrometers (WDS) and a JEOL JXA-8800R instrument at Nagoya University, Japan. The analytical conditions employed for quantitative analysis of silicates at Rice University were set to 15 kV acceleration voltage, 20 nA beam current, ca. 300 nm beam size. Analytical conditions at Nagoya University were set to 15 kV accelerating voltage, 12 nA beam current, and ≤5 μm beam size. One sample was measured at the University of Houston using a CAMECA SX-50 at 15 kV acceleration voltage and 20 nA beam current, and beam size ≤5 μm.

4.2. Trace Elements and REEs Analysis

Laser ablation inductively coupled plasma mass spectrometry (LA-ICP-MS) analyses of clinopyroxenes from the peridotite samples were accomplished using a Thermo-iCAP Q quadrupole mass spectrometer (Thermo

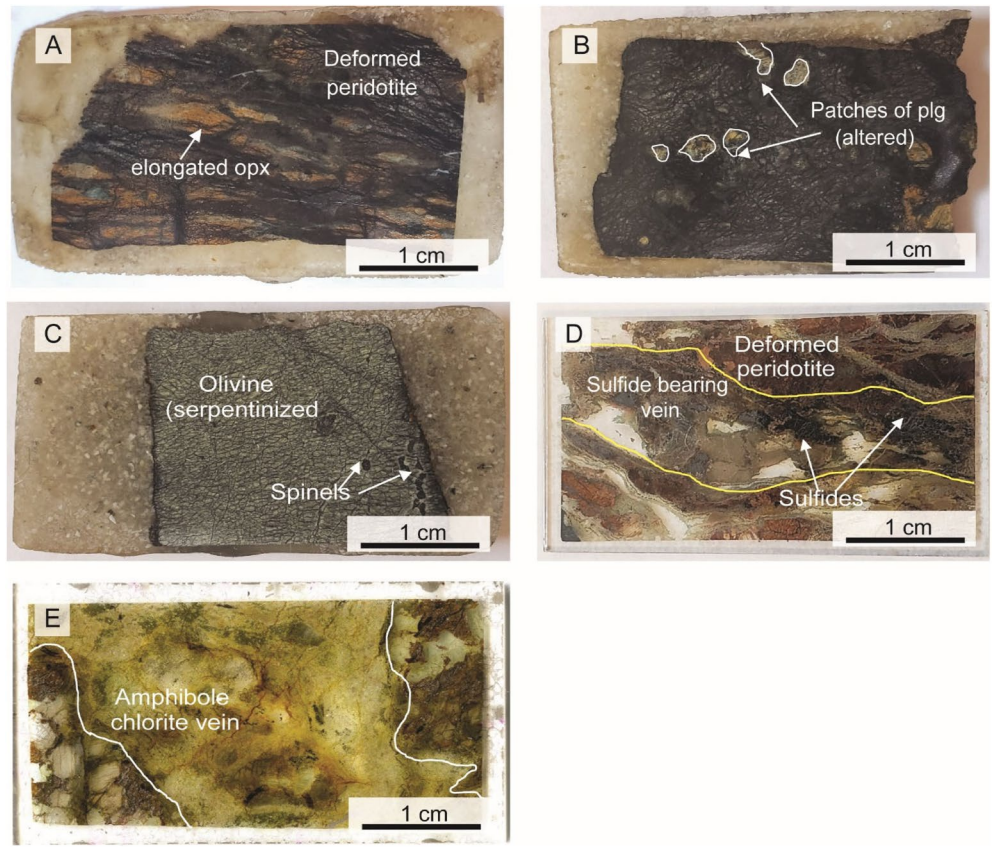

Figure 2. Photographs of billets and thin sections of representative samples. (a) Dry peridotite containing elongated porphyroclasts of orthopyroxene along foliation planes. (b) Melt reacted peridotite containing patches of altered plagioclase marked by the white dotted line. (c) Dunite sample that has serpentinized olivine and spinel. (d) Sulfide vein within peridotite where the sulfide bearing vein is marked by the dotted line. (e) Zircon-apatite bearing chlorite-amphibole vein that cuts across peridotite.

Scientific, Bremen, Germany) coupled with a New Wave/ESI 193 nm laser ablation system (Elemental Scientific Lasers, Huntingdon, UK) at the University of Arkansas Trace Element and Radiogenic Isotope Laboratory (TRAIL). Laser ablation analyses utilized a 50 μm laser spot diameter, 10 Hz repetition rate over 20 s, laser fluence of ≈4.3 J/cm^2, and the application of a He carrier gas flow rate of 0.800 L/min. Instrumental settings were adjusted to maintain UO and ThO <1.0%. The standard NIST 612 was used for calibration with ^{43}Ca as the internal standard in all analyses. Standards NIST 610 and NIST 612 were measured prior to and at the end of each analytical session and were bracketed once more after each set of 10 analyses during the analytical run. The investigated elements include the rare-earth elements (REEs), Sr, Y, Zr, Nb, Cs, Ba, Hf, Pb, Th, and U. Data reduction was carried out using the Iolite v4.4.3 software package (Iolite, Melbourne, Australia) (Paton et al., 2011) and the Trace Element data reduction scheme.

5. Results

5.1. Mineral Major Element Chemistry

Major element compositions of silicates (orthopyroxene, clinopyroxene, amphibole) and spinels are listed in Tables S1–S3 of Supporting Information S1.

5.1.1. Pyroxenes

The orthopyroxenes are enstatite in composition. The Mg# (Mg# = Mg/(Mg + Fe) mol%) ranges between 0.88 and 0.94 and Cr# (Cr# = Cr/(Cr + Al) mol%) up to 0.2. In a Mg#- Al_2O_3 diagram the orthopyroxenes mostly plot

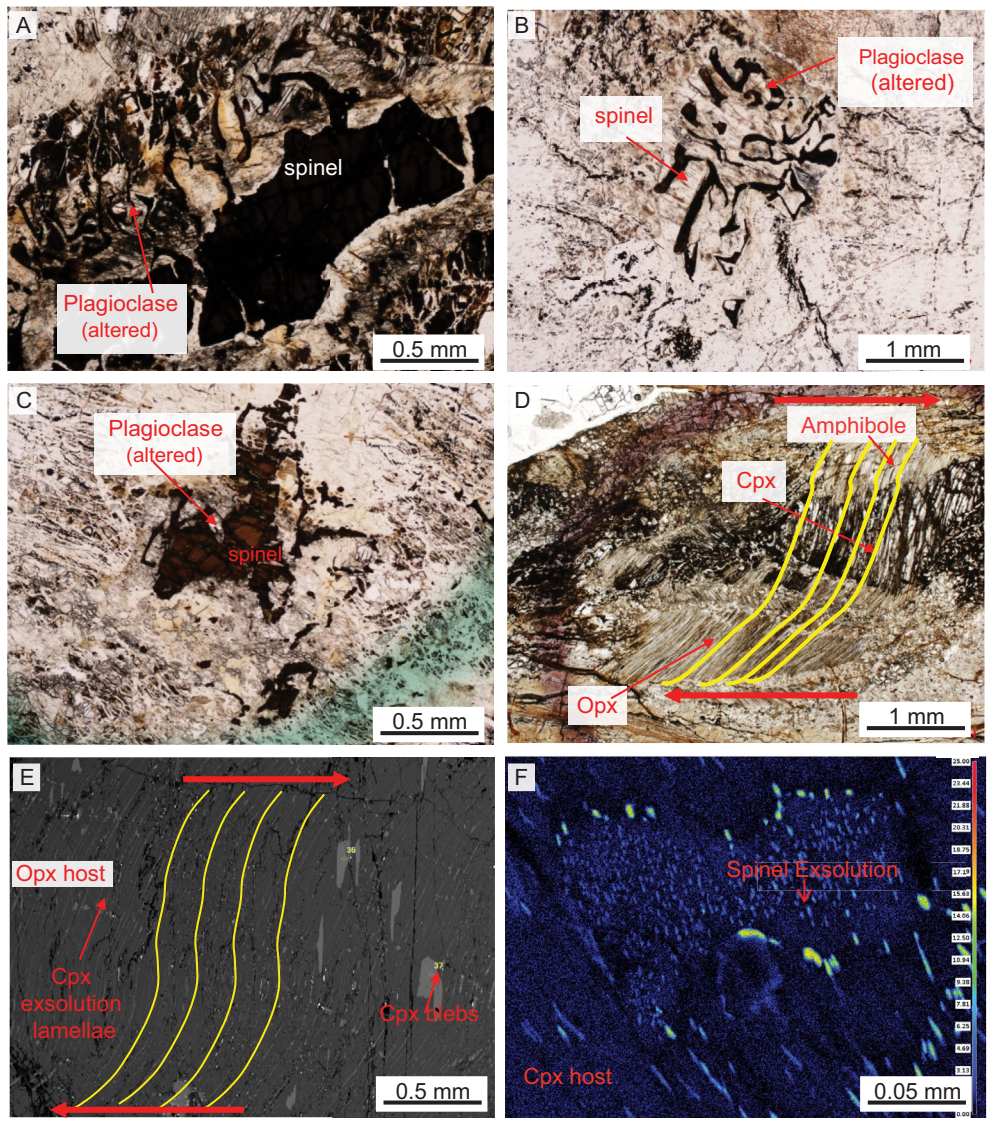

Figure 3. Photomicrographs, back scattered electron (BSE) image and X-Ray elemental map of mineral phases and deformation fabrics. (a) Holly leaf like mantle spinels that are replaced by plagioclase (altered) along its boundary. (b) Intergrowth between spinels and plagioclase (altered). (c) Altered plagioclase as along the boundary of spinels. (d) Mylonitized and deformed fabrics in mantle pyroxenes. The yellow dotted lines define the deformation planes and the arrows mark the shear direction. (e) BSE image shows the exsolution lamellae of clinopyroxene (cpx) and presence of cpx blebs in a host orthopyroxene (opx), a deformation plane can be defined from the exsolution lamellae. (f) X-Ray elemental map for Chromium shows exsolution of Cr rich oxides in a cpx host.

in the field of abyssal peridotites (Lian et al., 2016; Pagé et al., 2008) (Figure 4a; Table S1 in Supporting Information S1). Some of the orthopyroxenes have lower Al_2O_3 content and plots outside the field of abyssal peridotites.

The clinopyroxenes are diopside to chromium-rich diopside in composition (Cpx data; Table S1 in Supporting Information S1). They are present as individual mineral grains and as exsolutions lamellae and blebs in orthopyroxene. Their Mg# ranges between 0.90 and 0.95, their Cr# ranges between 0.08 and 0.32 and they contain up to 0.50 wt% TiO_2 (Figures 4b and 4c; Table S1 in Supporting Information S1). Exsolution of chromium-bearing oxides were found in some of the clinopyroxene grains. The clinopyroxenes exhibit a wide compositional range in terms of their Mg# and Al_2O_3 content. The average TiO_2 wt% versus Na_2O wt % plot (Figure 4c) shows that most of the samples fall in along a partial melting trend (Hellebrand et al., 2002) although there is a scatter toward higher Na_2O values at lower TiO_2 wt% for some samples.

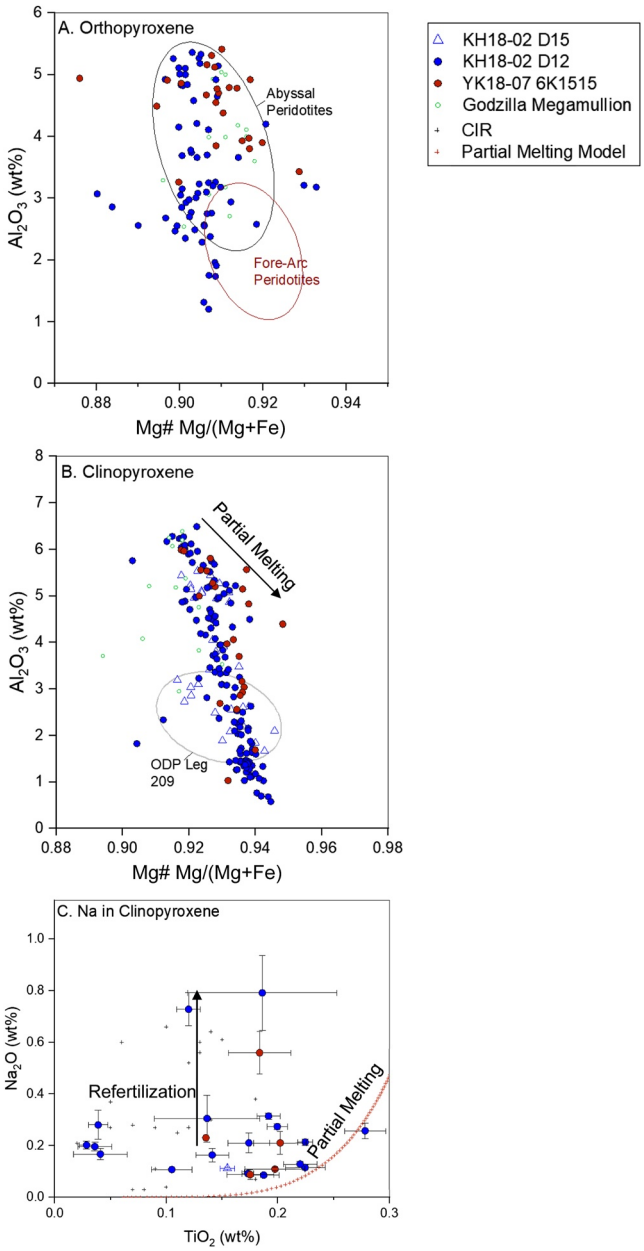

Figure 4. Major element compositional variation of mantle silicates in the peridotites (a) Mg# versus Al_2O_3 wt% for orthopyroxenes. The fields of fore-arcs and abyssal peridotites are from Pagé et al. (2008) (b) Clinopyroxene Mg# versus Al_2O_3 wt%. For comparison the compositional field of highly refractory peridotites from the Mid Atlantic Ridge (ODP leg 209) is marked by the gray ellipse (Seyler et al., 2007); Godzilla Megamullion data from Ohara et al. (2003). (c) Clinopyroxene TiO_2 wt% versus Na_2O wt%; data from Hellebrand et al. (2002).

5.1.2. Two-Pyroxene Geothermometer

Equilibration temperatures for mantle phases were calculated using the two-pyroxene geothermometers, considering that orthopyroxene and clinopyroxene (calcic diopside) were in equilibrium at upper mantle conditions (Bertrand & Mercier, 1985; Brey & Köhler, 1990). For calculation of the temperature, homogeneous pyroxene grains and areas that did not exhibit exsolution were chosen. At pressures ranging between 1.5 and 2 (kbars), the calculated equilibrium temperature ranges from 860 to 1140°C (Bertrand & Mercier, 1985), 820–1100°C (Taylor, 1998) and between 1140 and 1200°C (Brey & Köhler, 1990). These calculated temperatures are well within the ambient temperature of the mantle. The results were compared using REE in two-pyroxene thermometer for mafic and ultramafic rocks (Liang et al., 2013). This thermometer yields temperatures between 1025 and 1491°C. The temperatures from REE in pyroxene thermometer are generally about 150–200° higher than the major element thermometer. This discrepancy could be a result of the difference in diffusion rate and closure temperature between the +2 and +3 cations in the pyroxenes (Liang et al., 2013).

5.1.3. Spinel

The Cr# in spinels shows a wide range of composition from 0.20 to 0.63 mol% and Mg# ranges from 0.15 to 0.73 mol% and TiO_2 up to 0.26 wt% in the peridotites where plagioclase is present (Figures 5a and 5b). The TiO_2 content of the spinels goes up to 0.46 wt% (Spinel data Table S1 in Supporting Information S1) in some of the peridotites which have been crosscut by late-stage veins. The spinels in these veins have Cr# as high as 0.81 mol% and TiO_2 up to 0.62 wt% (Figures 5a and 5b). Concentric normal zoning (Dien et al., 2019; Mg-Al rich core and Cr-Fe^{2+} rich rim) is observed in spinel grains from sites KH18-2-D12 and YK18-07 6K1515. (Heterogeneous spinels; Table S2 in Supporting Information S1). These zoned spinels are present in the dry peridotite samples (Figure 6). The boundaries of these spinels are also marked by intergrowths with altered/metasomatized silicates (chlorite and amphibole).

5.1.4. Amphiboles

Brown-green pleochroic and colorless amphiboles are found in most of the samples, texturally replacing clinopyroxene (Figure 3d) and in leucocratic veins (Figure 2e). Most of the replacement amphiboles plot in the Edenite-Pargasite field (Leake et al., 1997) with a few crystals in the Edenite and Hornblende fields (Amphibole data; Table S3 in Supporting Information S1). These amphiboles also coincide generally in composition with the magmatic amphiboles from the gabbros of the Mado Megamullion (Basch et al., 2020) (Figure 7a). The amphiboles can be chemically distinguished between vein and replacement types based on the distribution of TiO_2 and Cr_2O_3 weight %. The composition of the amphiboles in the veins is similar to the compositions of both the vein amphiboles and magmatic amphiboles from the Mado gabbros (Basch et al., 2020). The replacement amphiboles are lower in TiO_2 and have higher Cr_2O_3 content than the amphiboles in the veins (Figure 7b). This would be consistent with a common origin, whereby the replacive amphiboles inherit immobile Cr from their host clinopyroxene.

5.2. Trace Elements and REE in Clinopyroxenes

Trace elements and REEs were analyzed in clinopyroxenes in the peridotites. The concentration of the REEs (mg/l) in clinopyroxenes is listed in Table S4 of Supporting Information S1. Chondrite-normalized REE plots show that the clinopyroxene porphyroclasts from samples that do not exhibit deformation features show an

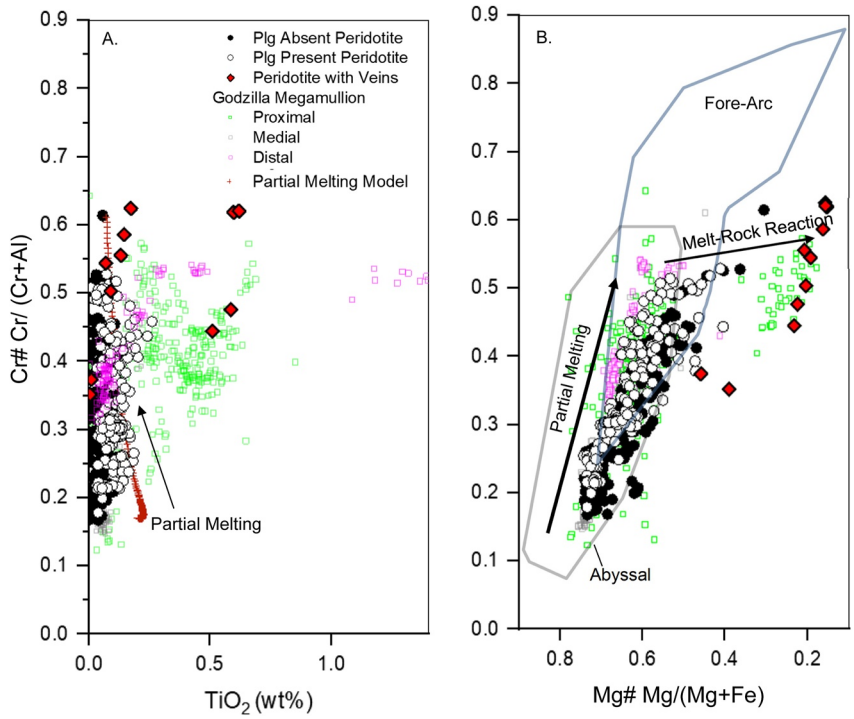

Figure 5. (a) Cr# versus TiO_2 content of spinels from YK 18-07, KH 18-02 residual peridotites, melt-reacted peridotites, and veined peridotite samples. (b) Cr# versus Mg# of spinels from YK 18-07, KH 18-02 peridotites, dunites, and veined peridotite samples from the Mado Megamullion. Proximal, medial and distal region of the Godzilla Megamullion from Loocke et al. (2013).

LREE-depleted trend (Figure 8a). This LREE depleted trend is similar to those reported from depleted abyssal peridotites generally (Dick, 1989; Dick et al., 1984; Johnson et al., 1990; Michael & Bonatti, 1985). Simple melting models produce extreme LREE depletion trends and do not explain the inflection of LREEs seen in these residual clinopyroxenes (Figure 8a), also commonly observed in REE patterns from abyssal peridotite clinopyroxenes.

Clinopyroxenes from the deformed peridotites or within deformed lamellae exhibit a flat REE pattern with a negative Eu anomaly (e.g., Figure 8a; enriched clinopyroxene). Similar REE patterns occur in the melt-impregnated peridotite samples of the Mariana Trough (Ohara et al., 2002) and the Parece Vela Rift (Ohara et al., 2003).

6. Discussion

6.1. Partial Melting

The spinels from the Mado peridotites plot within the normal range of abyssal peridotites (Dick & Bullen, 1984). The wide compositional range of spinels in terms of the Cr# suggests that the Mado mantle has undergone variable degrees of partial melting (Figures 5a and 5b) (Hellebrand et al., 2001). The presence of dunites and peridotites from the same dredge location indicates heterogeneous extraction, transport and reaction of melt (Kelemen et al., 1995; Niu, 1997). The heterogeneous spinels with increase in Cr toward the boundary (Figure 6) could be related to partial melting that removes Al^{3+} and increases Cr^{3+} in the residue (Dick & Bullen, 1984; Saumur & Hattori, 2013) at increasing degree of melting. The spreading rate and degree of melting are related (Niu & Hékinian, 1997), so initiation of normal detachment faulting after ca. 19 Ma might be related to a decrease in spreading rate to 30 mm/y (Okino, 2015) which resulted in an increase in the final depth of melting beneath the Shikoku Basin spreading axis.

The degree of partial melting can be estimated from the composition of spinels. A recent study has indicated that spinels can also act as a sink of fluid mobile elements and act as a tracer of metasomatic processes (Dien et al., 2019). We estimate the degree of partial melting from the major element composition of mantle spinels

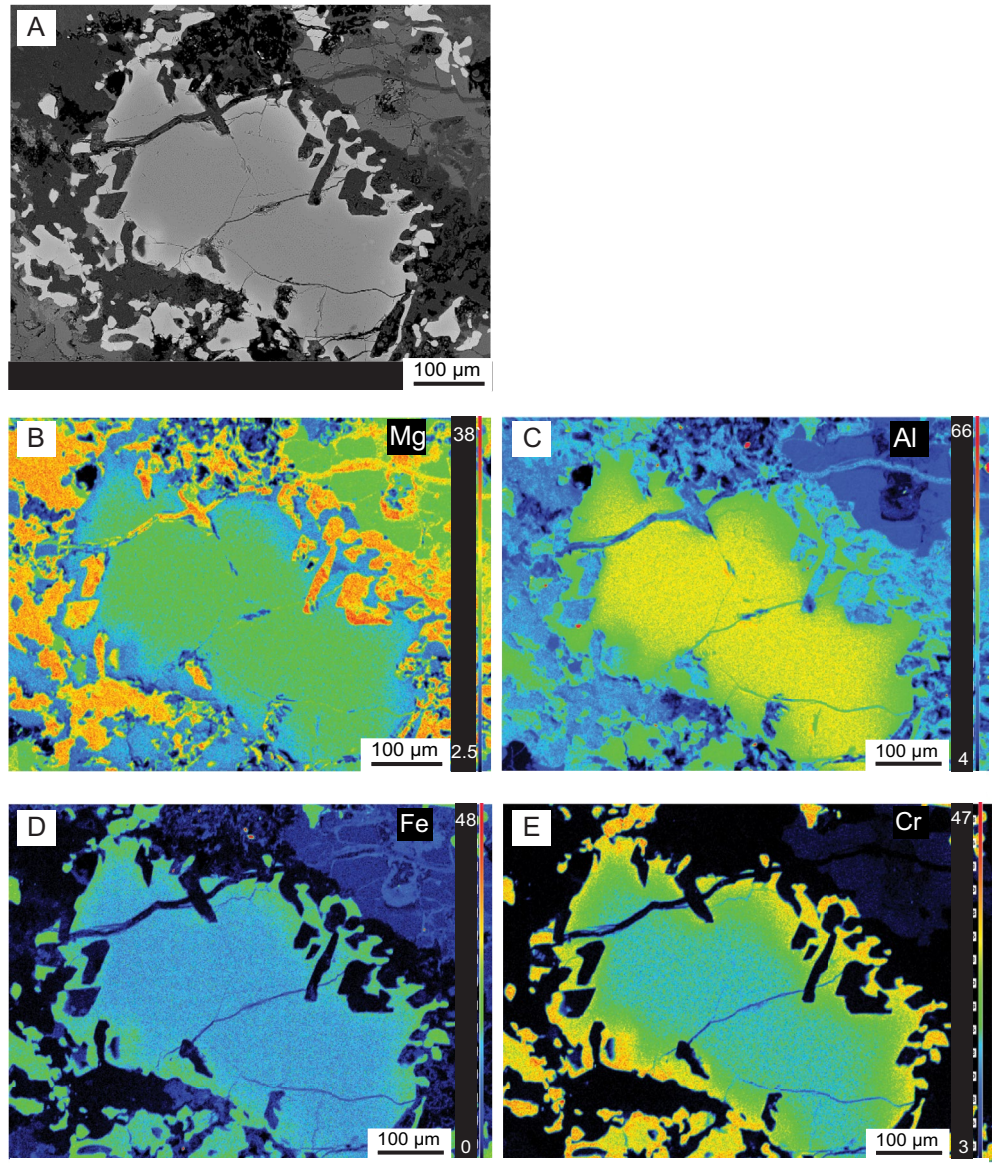

Figure 6. Back scattered electron (BSE) and X-Ray elemental maps for heterogeneous spinels. (a) BSE image with darker core and brighter boundary. (b–e) Mg-Al rich core and Fe-Cr rich boundary in the heterogeneous spinels.

(Dick & Bullen, 1984; Hellebrand et al., 2001). To model the degree of partial melting we ran a series of models using pMELTS (Ghiorso & Sack, 1995; Ghiorso et al., 2002) in the spinel stability field. We selected a Depleted MORB Mantle (DMM) composition (Workman & Hart, 2005) as the starting material. We sequestered 0.18 wt% Cr_2O_3 from the DMM composition to account for the lack of a solution model for Cr in pyroxene of MELTS. This was based on the modal abundance of clinopyroxene in DMM (Workman & Hart, 2005) and the distribution coefficients between minerals and melt during mantle melting (Roux et al., 2015). We melted this modified DMM adiabatically in the spinel stability field starting at 18 kbar until the base of the crust at 2 kbar. The starting temperature of the model was taken as 1350°C. The composition of the peridotite spinels could be reproduced by a range of 7%–21% partial melting. This agrees closely with Hellebrand et al. (2001)'s empirical calibration (degree of partial melting ranges from 6.28% to 17.66%) for the range of Cr# for the Mado Megamullion spinels (Figure 5a).

Clinopyroxene and orthopyroxene compositions plot in the range of abyssal peridotites, while the samples with lower proportion of clinopyroxenes have a higher Mg# and lower Al_2O_3 content and are comparable to the most

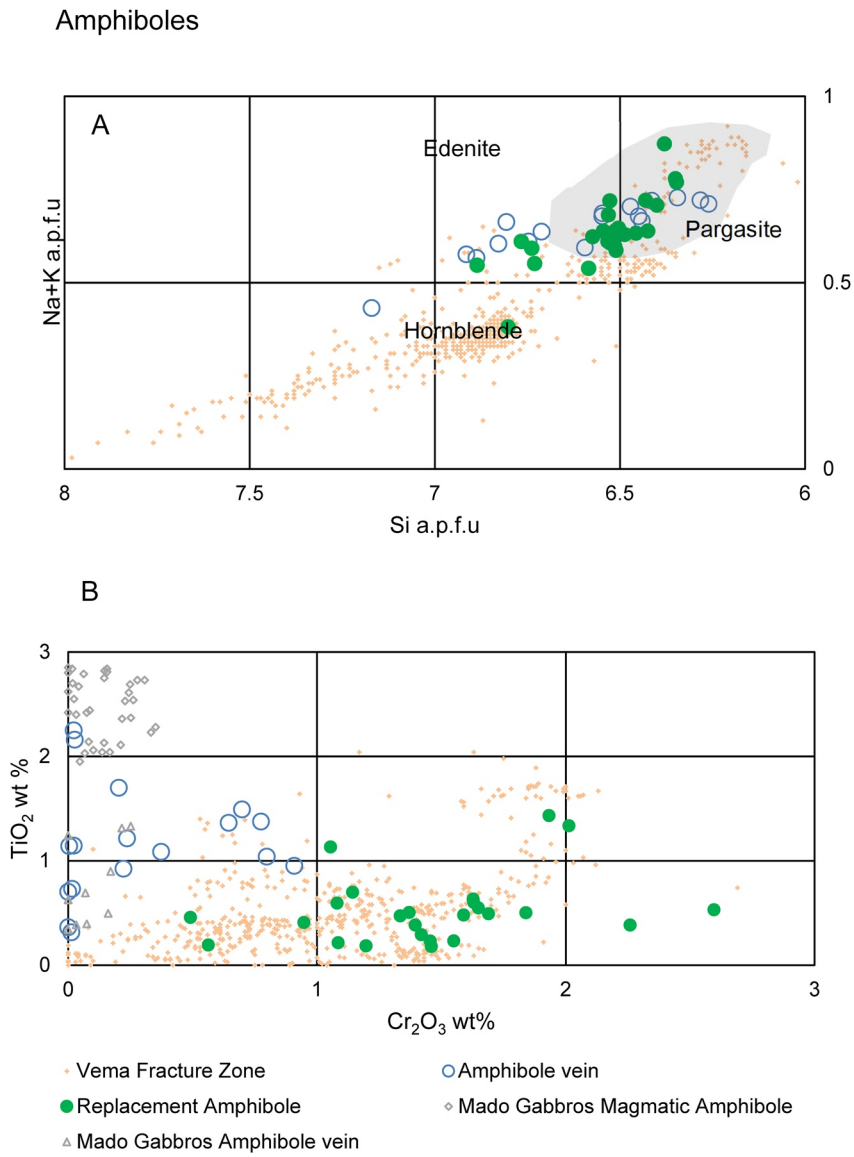

Figure 7. (a) Si a.p.f.u versus Na + K a.p.f.u indicates that most of the amphiboles plot in the magmatic amphibole field. The gray area is the field of magmatic amphiboles in the gabbros of the Mado Megamullion (Basch et al., 2020). The compositions of the Vema Fracture Zone amphiboles are from Cipriani, Bonatti, Brunelli, Ligi (2009) and Cipriani, Bonatti, Seyler, et al. (2009). (b) Cr_2O_3 wt% versus TiO_2 wt% plot for amphiboles where the replacement amphiboles have higher Cr_2O_3 wt% and lower TiO_2 wt% content than the amphibole in the veins.

depleted abyssal peridotites (Figures 4a and 4b). The composition of these refractory clinopyroxenes from the Mado Megamullion coincides with the composition of the highly refractory clinopyroxenes from the Mid-Atlantic Ridge, Ocean Drilling Program (ODP) Leg 209 Site 1274 (Seyler et al., 2007). The clinopyroxene compositions of peridotites reflect the degree of depletion by melting from fertile to depleted peridotites (Dick et al., 1984) leading to very refractory compositions (Johnson et al., 1990). The presence of fertile to melt-depleted peridotites and the compositional variability of spinels and silicates suggests that the Mado mantle has undergone variable degrees of melt depletion. The REE trends (discussed below) of the clinopyroxenes fall within the compositional range of abyssal peridotites and do not exhibit the extreme signatures of depletion in REE reported from fore-arc regions.

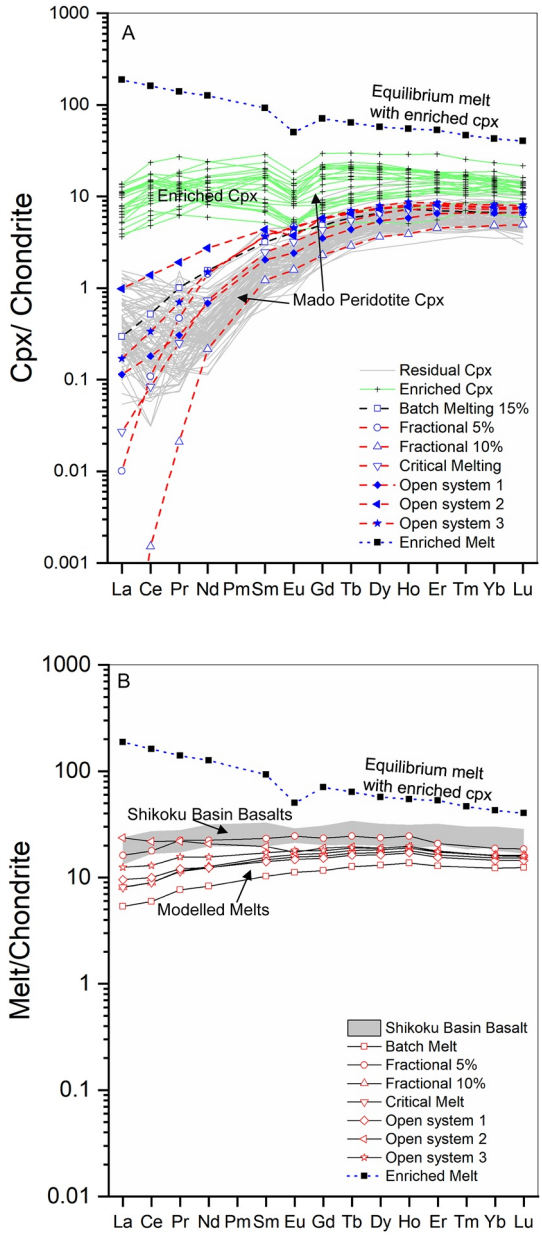

Figure 8. Chondrite normalized rare-earth element (REE) curves for clinopyroxenes and melt. (a) Residual and enriched clinopyroxenes composition of Mado peridotites. The dashed lines indicate the composition of the pyroxenes from batch melting, fractional melting, critical melting and open system melting processes. The enriched melt composition is a derived melt in equilibrium with an enriched clinopyroxene. The LREE enrichment trend is not explained by fractional melting alone and invokes the idea of an open system melting process. (b) REE Composition of accumulated melts from the different melting models (indicated by red symbols). The shaded area denotes the compositional filed of Shikoku basin basalts (Ishizuka et al., 2009). The open systems 2 and 3 closely approximates the composition of the basalts.

6.2. Melt Stagnation and Reaction

Plagioclase is present in 30% of the Mado peridotites, pseudomorphously replaced either as rims on spinel or as symplectic intergrowths (Figures 3a–3c). Fresh plagioclase is also found in some samples (). The widely accepted mechanisms for the formation of plagioclase-bearing peridotites are the following: (a) re-equilibration of an ascending mantle from the spinel stability field to the plagioclase stability field (Frost, 1976; Hamlyn & Bonatti, 1980) or (b) a melt-rock reaction mechanism driven by the impregnation of a melt into the residual peridotite (Dick, 1989; Dick & Bullen, 1984; Rampone et al., 2020). The spinels associated with the plagioclase-bearing peridotites exhibit an elevated content in TiO_2 and a wide range of composition in terms of spinel Cr#. The proportion of plagioclase-bearing lithologies and the extent of plagioclase impregnation is less than documented in the proximal region of the Godzilla Megamullion (Loocke et al., 2013). The presence of plagioclase and the TiO_2 content in spinels are used as an indicator of melt stagnation and reaction and a cut off at 0.12 wt% (Dick et al., 2010; Cannat et al., 1990; Loocke et al., 2013; Tartarotti et al., 2002) is generally used to distinguish residual peridotites from melt-reacted peridotites (Loocke et al., 2013; Ohara et al., 2003; Sanfilippo et al., 2013). The TiO_2 content of the spinels from the plagioclase-bearing peridotites ranges up to 0.26 wt%, which is much less than the TiO_2 content of the spinels in plagioclase-bearing peridotites from the proximal region of the Godzilla Megamullion where the TiO_2 content reaches 1.56 wt%. The compositional range of spinels from the plagioclase-bearing peridotites in terms of their Cr# (0.18–0.53) and TiO_2 content (up to 0.26 wt%) coincides better with the compositional range of spinels from the distal region of the Godzilla Megamullion where Cr# ranges from 0.33 to 0.64 and TiO_2 up to 0.45 wt% (Loocke et al., 2013) (Figures 5a and 5b). Thus, the slightly elevated TiO_2 content (Figure 5a) in the associated spinels in the plagioclase-bearing peridotites indicates melt stagnation and melt-rock reaction, although the extent of these indicators is much lower than that seen in the proximal regions of the Godzilla Megamullion (Loocke et al., 2013).

The expected partial melting trend is observed for some of the samples in terms of the variation of TiO_2 and Na_2O content in clinopyroxenes while some samples have a much higher primary clinopyroxene Na_2O concentration than those calculated for partial melting trends at given TiO_2 values (Figure 4c). A similar feature was observed for residual peridotites from the Central Indian Ridge (CIR) and was termed the "sodium problem" (Hellebrand & Snow, 2003). Similar re-fertilization trends have also been studied in the Mid Atlantic Ridge (Brunelli et al., 2006). Partial melting would deplete the residue in Na which is more incompatible than Ti, as also seen in our partial melting model. The enrichment in Na in some samples could indicate re-fertilization of residual peridotites (Hellebrand et al., 2002).

6.3. Relationship Between Hydrous Melt Infiltration and Exhumation

At decreasing temperatures, the complete solid-solution of pyroxenes changes to a limited solid-solution. As a result, the pyroxenes equilibrated at higher temperatures tend to assume ordered structure of separate phases (Ca-rich Cpx and Ca-poor Opx) in the form of exsolutions at lower temperatures (Poldervaart & Hess, 1951). Similar exsolution textures have been observed in ophiolites where mantle upwelling to shallower depths resulted in the formation of exsolutions (Basch et al., 2019; Kirby & Etheridge, 1981; Rehfeldt et al., 2007; Xiong et al., 2020). Our geothermometric calculations indicate that the pyroxenes (porphyroclasts)

equilibrated at a range of temperatures. We do not observe systematic variation of temperatures between the deformed and undeformed peridotite. The geothermometric calculations and the presence of exsolutions suggest that the rocks that equilibrated at greater depths were emplaced at shallower depths because of exhumation of mantle rocks at a slow-spreading axis.

The reason for the presence of spinel exsolutions in pyroxene is not well constrained yet. A suggested mechanisms that in the case of no change in the oxygen framework, the spinel nuclei forms by the migration of cations from interstitial sites and tetrahedral sites (Okamura et al., 1976). Another possibility is a variation in the local oxidation state of the system. In the presence of magnetite and amphibole that consume O_2 and Fe^{3+} from the magmatic system, spinel may exsolve from the pyroxene structure (Zhu et al., 2018). The Mado peridotites have been crosscut by late-stage oxide-bearing amphibole-chlorite veins. The clinopyroxenes in the lherzolites contain amphiboles. Magmatic amphiboles are also ubiquitously present in the Mado gabbros (Basch et al., 2020). This indicates that a late-stage process of melt percolation may have played a significant role for the exsolution of spinels from the structure of pyroxenes (Cr-diopsides). The textural relationships between magmatic veins rich in amphiboles (considered as late-stage hydrous melts) and the deformed pyroxenes indicate that melt was present during the deformation history that promoted the exhumation of the peridotites to the seafloor. These melts could have played a significant role in promoting detachment. The presence of mylonitized fabrics along the exsolution lamellae (Figures 3d and 3e) also indicates that the peridotites underwent crystal-plastic deformation during the slow exhumation of the mantle (Hirauchi et al., 2021) and formation of the OCC in the slow-spreading back-arc Shikoku basin. Because these samples do not represent a time series (e.g., Brunelli et al., 2018; Cipriani, Bonatti, Brunelli, & Ligi, 2009; Cipriani, Bonatti, Seyler, et al., 2009) they provide no information about the secular evolution of the mantle.

6.4. Evolution in a Water-Rich Environment

The presence of the different types of amphiboles in peridotites suggests the presence of water, at least in the late stages of the formation of the OCC (Harigane et al., 2019; Zhang et al., 2021). It cannot be determined whether there was sufficient water in the system during melting to crystallize amphibole as a primary mantle phase. However, the presence of magnetite, ilmenite and other Ti-bearing oxides in the amphibole veins and their crosscutting relationship with the peridotites (Figure 2e) suggest strongly that these amphiboles crystallized from a melt rich in incompatible elements and water, injected to a mantle sequence at the boundary between ductile and brittle regime. High-temperature pargasitic amphiboles have been identified from abyssal peridotites from very few localities (Cipriani, Bonatti, Brunelli, & Ligi, 2009; Cipriani, Bonatti, Seyler, et al., 2009; Melson et al., 1967; Ohara et al., 2003; Seyler et al., 2004); most of the amphiboles documented in abyssal peridotites are tremolitic. Amphiboles studied from the Vema Fracture Zone range from tremolites to magnesio hornblendes and pargasites (Cipriani, Bonatti, Brunelli, & Ligi, 2009; Cipriani, Bonatti, Seyler, et al., 2009). The compositional similarity between the pargasitic amphiboles in the veins within the peridotites in this study and the magmatic amphiboles in the gabbros from the Mado Megamullion (Figures 7a and 7b) suggests that these amphiboles are genetically related. The higher Cr_2O_3 content in the replacement amphiboles (Figure 7b) could indicate a reaction of Cr-rich pyroxenes with hydrous mafic melt (hydrous melt that formed the Mado gabbros; see Basch et al., 2020) or late-stage deuteric fluids to form the Cr-rich amphiboles. High Cr_2O_3 bearing pargasitic amphiboles have been studied from the Vema Fracture Zone that formed by the action of mantle derived water rich fluids close to the ridge axis (Cipriani, Bonatti, Brunelli, & Ligi, 2009; Cipriani, Bonatti, Seyler, et al., 2009). Melts can be injected after ductile shearing along fracture zones in mid oceanic ridges by the interplay of shearing, rock rheology and melt accumulation (Brunelli et al., 2020). The presence of pargasitic amphiboles in peridotites from this study suggests that back-arc mantle could be hydrated/hydrous. Late stage metasomatic effects are seen often in mantle rocks and these amphiboles corresponds to the presence of hydrous components in the mantle (Basch et al., 2020; Seyler et al., 2004). It is also observed from in situ crystallization experiments that amphibole-bearing peridotites could form by reaction between lherzolites and hydrous partial melt (Wang et al., 2021). The replacement amphiboles from this study can be inferred to be reacted amphibole and this reaction product can lead to the hydration of the mantle in a back-arc environment. Amphiboles occurring in the Godzilla Megamullion peridotites (Ohara et al., 2003) have not yet been systematically studied, so it is not possible to say whether their occurrence or composition are consistent between the two complexes. It is possible that an increased influence of water-rich melts is a characteristic of back-arc abyssal peridotites as compared to those outcropping at mid-ocean ridges.

Table 2
Mineral/Melt Partition Coefficients Used in the Models

	Olivine[a]	Orthopyroxene[b]	Clinopyroxene	Spinel[c]
La	0.0002	0.0031	0.055[d]	
Ce	7E-05	0.004	0.0876[d]	0.0005
Pr			0.1318[d]	
Nd	0.00042	0.012	0.1878[d]	0.0008
Sm	0.0011	0.02	0.3083[d]	0.0009
Eu	0.0005		0.3638[d]	
Gd	0.0011	0.0065	0.4169[d]	0.0009
Tb			0.4645[d]	
Dy	0.0027	0.011	0.5034[d]	0.0015
Ho			0.5294[d]	
Er	0.0109	0.045	0.5437[d]	0.0045
Tm			0.5482[d]	
Yb	0.024	0.08	0.5453[d]	0.0045
Lu	0.02	0.12	0.5373[d]	
Rb	0.0003	0.0002	0.0004[b]	
Ba	5E-06	6E-06	0.0004[b]	
Th	5E-05	0.002	0.0059[b]	
U	0.00038	0.002	0.0094[b]	
Nb	0.0005	0.004	0.015[b]	
Ta	0.0005	0.004	0.015[b]	
K	2E-05	0.0001	0.001[b]	
Pb	0.003	0.009	0.012[b]	
Sr	4E-05	0.0007	0.091[b]	
Hf	0.0022	0.03	0.2835[b]	
Zr	0.005	0.0225	0.075[c]	0.05
Ti	0.008	0.0805	0.23[c]	0.1
Y			0.5219[d]	

[a]From Stracke et al. (2003). [b]From Salters and Stracke (2004). [c]From Sobolev and Shimizu (1992). [d]From Sun and Liang (2012).

Table 3
Modal Proportions of the Phases Used in the Models

	Initial mode[a]	Melt mode[b]	Crystallization mode[c]
Olivine	0.58	−0.3	0.7
Orthopyroxene	0.26	0.4	
Clinopyroxene	0.13	0.82	0.3
Spinel	0.03	0.08	

[a]Sobolev and Shimizu (1992). [b]Kinzler and Grove (1992). [c]Elthon (1992).

6.5. Evolution of the Depleted Clinopyroxenes

To model the trace element distribution in the most depleted clinopyroxenes, we have taken a DMM composition (Workman & Hart, 2005) as our starting mantle composition. We have modeled the trace elements and REEs using equations for equilibrium melting (Shaw, 1970) and fractional melting (Johnson et al., 1990). The partition coefficients between clinopyroxene and liquid is taken from the newer predictive model for partitioning of REE and Y between clinopyroxene and a basaltic melt (Sun & Liang, 2012) by least squares analysis of available partitioning data based on the lattice strain model (Blundy & Wood, 1994; Brice, 1975) at 1300°C. The partition coefficient of olivine (Stracke et al., 2003), orthopyroxene (Salters & Stracke, 2004) and spinel (Sobolev & Shimizu, 1992) is listed in Table 2. The initial mode (Sobolev & Shimizu, 1992), melting mode (Kinzler & Grove, 1992) and crystallization modes (Elthon, 1992) used for the models are listed in Table 3. Although the batch melting models depletes the LREEs less than the fractional melting models, batch melting does not reach the observed depletion in incompatible trace elements in residual peridotite clinopyroxenes even with 15% melt extraction (Figure 8a). Fractional melting, on the other hand, satisfies the REE depletion trend for most elements, except for the La-Ce enrichment commonly seen in ocean floor peridotites (Hellebrand et al., 2002; Johnson et al., 1990; Ohara et al., 2002) (Figure 8a).

To better understand the process we also used critical melting (Maaløe, 1982; Sobolev & Shimizu, 1992), where a residue of melting (α is the mass ratio of retained melt) is left behind in the pore spaces during partial melting and the REEs in the residual peridotites equilibrate with the melt. The critical melting model with $\alpha = 0.01$ and 10% fractional melting exhibits LREE enrichment as compared to the 10% fractional melting alone, but this still does not explain the higher LREE abundances in some of the residual clinopyroxenes.

6.6. Evolution of Enriched Signatures

The flat REE patterns in equilibrium with enriched melts from Mado clinopyroxene are associated with deformation and veining. Enrichment trends implies melt retention or open-system behavior (Brunelli et al., 2006, 2014; Hellebrand et al., 2002; Seyler et al., 2011). The enrichments of LREEs, MREE, Zr, and Sr observed in supra-subduction zone peridotites can be modeled by the influx of a slab derived fluid component to the melting wedge (Bizimis et al., 2000). The presence of the enriched clinopyroxenes in the deformed peridotites in our study suggests the presence of an enriched melt. We therefore employed the open-system modeling mechanism (Dick et al., 1984; Ozawa & Shimizu, 1995). To estimate the composition of enriched melt, we used the enriched clinopyroxene composition from a typical deformed peridotite sample (KH18-2-D12-R17) and calculated the equilibrium melt composition using the partition coefficient between cpx and melt ($D^{cpx/liq}$) (Salters & Stracke, 2004; Sun & Liang, 2012). This composition compares closely to that of the hypothetical enriched component in the Mariana Trough peridotites (Ohara et al., 2002). We used this melt composition as the composition of the enriched metasomatic melt (Appendix B). With a degree of fractional melting ranging from 7% to 10% and $\alpha = 0.01$ and influx rate (β) of 0.01, the clinopyroxenes in the residue exhibit more enrichment compared to the fractional or critical melting models (Figure 8a). After running the same model at a higher enriched melt influx rate ($\beta = 0.1$), more enriched LREE patterns could be reproduced in the clinopyroxenes. The clinopyroxenes modeled by the mechanisms describe above is given in Appendix A. The HREE trends are primarily controlled by the

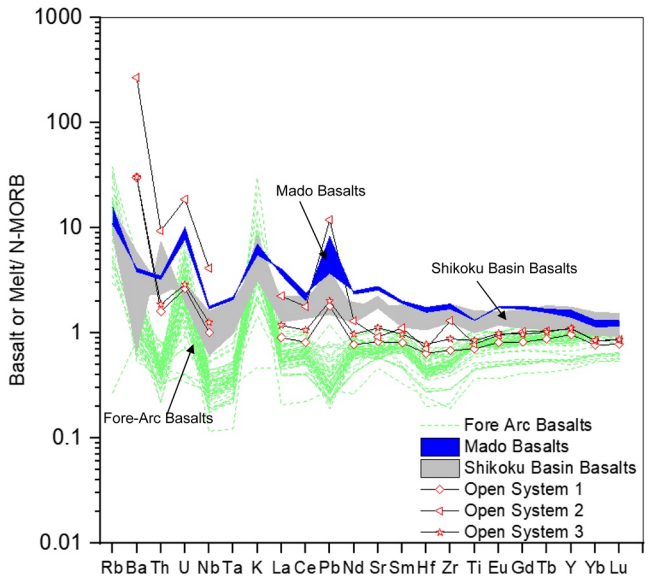

Figure 9. Multi-element spider diagram normalized to N-MORB (Sun & McDonough, 1989). The back-arc basalts from the Shikoku basin and Mado Megamullion shows distinct enrichment trends in comparison to fore arc basalts from the Izu-Bonin-Mariana arc. Our open system models for the accumulated melt compositions closely approximate the trends shown by the Shikoku basin basalts along with the enrichment trends in fluid mobile elements (Ba, U, and Pb).

degree of melting (F) and significant difference in the HREEs is not produced due to the melt fraction retained or the influx rate (β) of the LREE enriched melt (Ozawa & Shimizu, 1995). Although no significant change in the HREE pattern is observed in the fractional, critical or open system models, it is observed that the critical melting and the open-system melting processes produce a higher HREE abundance at the same degree of partial melting.

6.7. Modeled Accumulated Melts and Shikoku Basin Basalts

Shikoku Basin back-arc basalts (Ishizuka et al., 2009) are enriched in LREE compared to N-MORB (Sun & McDonough, 1989). We modeled the accumulated melt compositions (Appendix B) from batch melting, fractional melting, critical melting and open-system melting mechanisms (Figure 8b). Our models indicate that the compositions of the accumulated melts from the fractional melting (10%), batch melting, critical melting, and open system 1 with enriched melt influx rate (β) of 0.01, degree of melting (F) 10% and melt porosity (α) = 0.01 (Figure 8b) processes do not show the enrichment documented in the Shikoku Basin basalts (Ishizuka et al., 2009). Only the accumulated melt compositions from the open system 2 process (with a higher enriched melt influx rate (β) of 0.1, $\alpha = 0.01$ at $F = 10\%$) and fractional melting (5%) shows a compositional similarity with the Shikoku Basin basalts. The open system 3 ($F = 7\%$, $\alpha = 0.01$, $\beta = 0.01$) plots slightly lower than the compositional field of the Shikoku Basin basalts (Figure 8b). In the extended spider diagram (Figure 9) it is seen that open system 2 estimates a higher proportion of fluid mobile elements (Ba, U, and Pb) than that seen in the Shikoku Basin basalts as well as the Mado basalts (Basch et al., 2020). The composition predicted by open system 3 plots in the field of the Shikoku Basin basalts and closely estimates the analyzed trace element compositions (Figure 9).

6.8. Tectonic Implications

The enrichment seen in the Shikoku Basin basalts was predicted by the open system 2 model where the proportion of the influxing melt was high ($\beta = 0.1$). The feasibility of this melt influx rate is not well constrained in a back-arc spreading environment. The open system model 3 with 7% degree of melting and melt influx rate $\beta = 0.01$ closely resembles the composition of the Shikoku Basin basalts. This rate of melt influx compared to the open system 2 seems to be a more realistic scenario as the Mado Megamullion formed at the final stages of back-arc spreading when the melt production rate decreased leading to moderate melt-rock reaction or re-fertilization of the residual clinopyroxenes which are also consistent with the melt-rock reaction textures and chemistry seen in the Mado spinels. The higher enrichment trends seen in the Mado Megamullion basalts in terms of the fluid-mobile elements respect to those predicted by our open system 3 model could be produced by the influx of a hydrous melt rich in fluid-mobile elements (Gale et al., 2013). The basalts from the Izu-Bonin-Mariana fore-arc region display distinctive geochemical signatures with an overall depletion in trace elements and REEs (Figure 9) compared to back-arc basalts or MORBs (Shervais et al., 2019). These depleted signatures reflect a higher degree of partial melting in a fore-arc region. A two-stage melting process was suggested (Shervais et al., 2019) where shallow melting at higher potential temperatures (due to the presence of a hotspot) of an already depleted source led to these depletions. Thus, the source mantle in a back-arc spreading environment and a fore-arc region could be different. The domal structures that we see in OCCs have been discovered to have formed along slow- to ultraslow-spreading axes in the Southwest Indian Ridge, Mid-Atlantic Ridge, as well as back-arc basins. Initial interpretation of the recovery of serpentinized peridotites was that the exhumation of the mantle rock was fault driven in a magma-starved condition (Tucholke et al., 1998). However, ODP and Integrated Ocean Drilling Program (IODP) holes from the Atlantis Bank in the Southwest Indian Ridge and the Atlantis Massif in the Mid-Atlantic Ridge has recovered thick layers of gabbroic rocks (Dick, Kvassnes, et al., 2019; Dick, MacLeod, et al., 2019;

Godard et al., 2009; Ildefonse et al., 2007). It has been suggested from numerical modeling that long-lived detachment faults could be formed by extension accommodated by magmatic accretion (Tucholke et al., 2008).

Hydrous open-system magmas are to be expected as a component in the petrogenesis of peridotite from back-arc basins. Their occurrence sets back-arc peridotites apart from the majority of mid-ocean ridge peridotites, where primary or near-primary amphibole is extremely rare, and the contribution of enriched metasomatic fluids are minor.

7. Conclusions

The deformation-related textures and chemistry of associated spinels and silicates suggest that the Mado Megamullion peridotites are residues of melting and melt-rock interactions with hydrous basaltic liquids probably equivalent to primitive back-arc basin basalts. The abundance of residual peridotites and the compositions of primary silicates and spinels that fall in the range of global abyssal peridotites suggest a relatively wide range of degrees of partial melting. The elevated content of TiO_2 in spinels from the plagioclase-bearing peridotites and the presence of residual and melt-reacted peridotites from the same dredge site requires the involvement of melt stagnation or melt-rock reaction. The composition of the spinels from the Mado Megamullion is similar to those of peridotites from the distal region of the Godzilla Megamullion, and the extent of melt stagnation is lower than the proximal Godzilla Megamullion. Ten percent fractional melting can approximate the MREE-HREE compositions of the most depleted peridotite clinopyroxenes. The multiple generations of amphiboles suggest the involvement of water at different stages of exhumation of the OCC. The compositional similarity between the amphiboles in the veins to the magmatic amphiboles suggests a genetic relationship between them. Back-arc mantle could be hydrated by reaction of the peridotites with hydrous melt. Exsolution between orthopyroxene, clinopyroxene and Cr-bearing oxides suggests a change in oxygen fugacity and water content in the infiltrating melt compared to the host peridotite. The flat REE pattern of the clinopyroxenes in the deformed peridotites and along deformation planes indicates the presence of an enriched melt that was in equilibrium with these clinopyroxenes. The moderate enrichment "inflection" of LREEs in the residual clinopyroxenes cannot be reproduced by fractional melting alone and rather indicates the involvement of an enriched melt that reacted with the residual peridotite clinopyroxenes. Our open system models with moderate degrees of melting (between 7%-10%) closely approximates the composition of the residual clinopyroxenes with moderate influx rates of $\beta = 0.01$ and melt porosity $\alpha = 0.01$. The composition of the accumulated melts from these open system models also approximates the composition of Shikoku basin and Mado basalts. The enrichment in fluid mobile elements in the back-arc basalts with respect to N-MORB indicates the presence of hydrous melts in the system that acted as carriers of these fluid-mobile elements. We infer that reaction of refractory mantle with enriched hydrous melts played an important role in the evolution of the Mado Megamullion mantle peridotites and crustal basalts in the back-arc spreading system.

Appendix A: Composition of Modeled Clinopyroxenes Normalized to Chondrite (McDonough & Sun, 1995)

	Batch melting	Fractional 5%	Fractional 10%	Critical melting	Open system 1	Open system 2	Open system 3
La	0.29	0.01	0.00	0.03	0.11	0.98	0.17
Ce	0.52	0.11	0.00	0.08	0.18	1.39	0.33
Pr	1.01	0.47	0.02	0.25	0.31	1.91	0.70
Nd	1.55	1.43	0.22	0.73	0.68	2.73	1.49
Sm	3.17	3.74	1.22	2.45	2.03	4.35	3.66
Eu	4.06	4.67	1.58	3.21	2.41	3.73	4.53
Gd	4.84	5.64	2.29	4.31	3.49	5.73	5.74
Tb	5.88	6.71	2.89	5.45	4.36	6.54	6.97
Dy	6.56	7.47	3.64	6.51	5.40	7.30	7.90
Ho	7.25	8.09	3.89	7.19	5.83	7.74	8.65

	Batch melting	Fractional 5%	Fractional 10%	Critical melting	Open system 1	Open system 2	Open system 3
Er	6.97	7.87	4.52	7.39	6.52	8.16	8.47
Tm							
Yb	6.69	7.58	4.80	7.26	6.59	7.66	8.08
Lu	6.66	7.51	4.90	7.28	6.65	7.56	8.01

Note. Critical melting $F = 0.10$; $\alpha = 0.01$. Open system 1 $F = 0.10$; $\alpha = 0.01$; $\beta = 0.01$. Open system 2 $F = 0.10$; $\alpha = 0.01$; $\beta = 0.1$. Open system 3 $F = 0.07$; $\alpha = 0.01$; $\beta = 0.0.01$.

Appendix B: Composition of Calculated Influxed Melt and Modeled Accumulated Melts Normalized to Chondrite (McDonough & Sun, 1995)

	Enriched melt	Batch melt	Fractional 5%	Fractional 10%	Critical melting	Open system 1	Open system 2	Open system 3
La	187.98	5.36	16.19	8.10	8.09	9.56	23.71	12.47
Ce	161.32	5.92	17.79	8.97	8.93	9.97	21.80	12.94
Pr	140.03	7.64	22.37	11.53	11.43	12.05	21.95	15.59
Nd	125.92	8.26	22.37	12.65	12.32	12.37	20.75	15.56
Sm	92.65	10.29	23.32	15.50	14.73	14.12	19.57	17.07
Eu	50.30	11.16	24.44	16.43	15.62	14.78	17.28	17.87
Gd	70.68	11.61	23.44	16.81	15.88	15.18	18.96	17.92
Tb	63.85	12.65	24.44	17.97	16.95	16.24	19.48	19.00
Dy	57.07	13.04	23.49	18.20	17.11	16.32	18.97	18.78
Ho	54.51	13.70	24.53	18.94	17.81	17.09	19.58	19.65
Er	53.18	12.82	20.83	17.30	16.28	15.50	17.72	17.38
Tm								
Yb	42.72	12.26	18.79	16.19	15.30	14.48	15.99	16.02
Lu	40.25	12.39	18.54	16.18	15.31	14.50	15.83	15.95

Note. Model parameters same as Appendix A.

Data Availability Statement

Major element composition data of spinels, orthopyroxenes and clinopyroxenes in Table S1 of Supporting Information S1 are also available online (https://doi.org/10.5281/zenodo.5033571).

Acknowledgments
The authors gratefully acknowledge the hard work of the RV Hakuho Maru (KH07-02, KH18-2) and R/V Yokosuka (YK18-07) crew and Shinkai 6500 pilots and staff. Dr. Gelu Costin gave insightful help with the Rice University electron probe facility. The authors also thank Dr. Barry Shaulis for his help with the LA-ICP-MS at the University of Arkansas. The careful reviews by Donna Blackman and Anna Cipriani, and editorial handling by Marie Edmonds improved the quality of this paper. This research was supported by the office of Department of Geology and Geophysics, Louisiana State University NSF award #1737031 to J. E. Snow, JSPS KAKENHI Grant number 18K13638 to K. Hirauchi and JP16H06347 to Y. Ohara.

References

Akizawa, N., Ohara, Y., Okino, K., Ishizuka, O., Yamashita, H., Machida, S., et al. (2021). Geochemical characteristics of back-arc basin lower crust and upper mantle at final spreading stage of Shikoku Basin: An example of Mado Megamullion. *Progress in Earth and Planetary Science*, *8*(1), 1–24. https://doi.org/10.1186/S40645-021-00454-3

Baines, G. A., Cheadle, M. J., Dick, H. J. B., Hosford Scheirer, A., John, B. E., Kusznir, N. J., & Matsumoto, T. (2003). Mechanism for generating the anomalous uplift of oceanic core complexes: Atlantis Bank, southwest Indian Ridge. *Geology*, *31*(12), 1105. https://doi.org/10.1130/G19829.1

Basch, V., Rampone, E., Borghini, G., Ferrando, C., & Zanetti, A. (2019). Origin of pyroxenites in the oceanic mantle and their implications on the reactive percolation of depleted melts. *Contributions to Mineralogy and Petrology*, *174*(12), 97. https://doi.org/10.1007/s00410-019-1640-0

Basch, V., Sanfilippo, A., Sani, C., Ohara, Y., Snow, J., Ishizuka, O., et al. (2020). Crustal accretion in a slow-spreading back-arc basin: Insights from the Mado Megamullion oceanic core complex in the Shikoku Basin. *Geochemistry, Geophysics, Geosystems*, *21*(11). https://doi.org/10.1029/2020gc009199

Bertrand, P., & Mercier, J. C. C. (1985). The mutual solubility of coexisting ortho- and clinopyroxene: Toward an absolute geothermometer for the natural system? *Earth and Planetary Science Letters*, *76*(1–2), 109–122. https://doi.org/10.1016/0012-821x(85)90152-9

Bizimis, M., Salters, V. J., & Bonatti, E. (2000). Trace and REE content of clinopyroxenes from supra-subduction zone peridotites. Implications for melting and enrichment processes in island arcs. *Chemical Geology*, *165*(1–2), 67–85. https://doi.org/10.1016/s0009-2541(99)00164-3

Blackman, D. K., Canales, J. P., & Harding, A. (2009). Geophysical signatures of oceanic core complexes. *Geophysical Journal International*, *178*, 593–613. https://doi.org/10.1111/j.1365-246X.2009.04184.x

Blackman, D. K., Cann, J. R., Janssen, B., & Smith, D. K. (1998). Origin of extensional core complexes: Evidence from the Mid-Atlantic Ridge at Atlantis fracture zone. *Journal of Geophysical Research: Solid Earth*, *103*(9), 21315–21333. https://doi.org/10.1029/98jb01756

Blackman, D. K., Ildefonse, B., John, B. E., Ohara, Y., & MacLeod, C. J. (2006). Expedition 304/305 Scientists. *Proceedings of the Integrated Ocean Drilling Program* (Vol. 304–305). https://doi.org/10.2204/iodp.-proc.304305.302006

Blackman, D. K., Ildefonse, B., John, B. E., Ohara, Y., Miller, D. J., MacLeod, C. J., et al. (2005). IODP Expeditions 304 and 305: Oceanic core complex formation, Atlantis Massif. *Scientific Drilling*, *1*, 28–31. https://doi.org/10.2204/iodp.sd.1.05.2005

Blundy, J., & Wood, B. (1994). Prediction of crystal-melt partition coefficients from elastic moduli. *Nature*, *372*(6505), 452–454. https://doi.org/10.1038/372452a0

Brey, G. P., & Köhler, T. (1990). Geothermobarometry in four-phase lherzolites II. New thermobarometers, and practical assessment of existing thermobarometers. *Journal of Petrology*, *31*(6), 1353–1378. https://doi.org/10.1093/petrology/31.6.1353

Brice, J. C. (1975). Some thermodynamic aspects of the growth of strained crystals. *Journal of Crystal Growth*, *28*(2), 249–253. https://doi.org/10.1016/0022-0248(75)90241-9

Brunelli, D., Cipriani, A., & Bonatti, E. (2018). Thermal effects of pyroxenites on mantle melting below mid-ocean ridges. *Nature Geoscience*, *11*(7), 520–525. https://doi.org/10.1038/s41561-018-0139-z

Brunelli, D., Paganelli, E., & Seyler, M. (2014). Percolation of enriched melts during incremental open-system melting in the spinel field: A REE approach to abyssal peridotites from the Southwest Indian Ridge. *Geochimica et Cosmochimica Acta*, *127*, 190–203. https://doi.org/10.1016/j.gca.2013.11.040

Brunelli, D., Sanfilippo, A., Bonatti, E., Skolotnev, S., Escartin, J., Ligi, M., et al. (2020). Origin of oceanic ferrodiorites by injection of nelsonitic melts in gabbros at the Vema Lithospheric Section, Mid Atlantic Ridge. *Lithos*, *368*, 105589. https://doi.org/10.1016/j.lithos.2020.105589

Brunelli, D., Seyler, M., Cipriani, A., Ottolini, L., & Bonatti, E. (2006). Discontinuous melt extraction and weak refertilization of mantle peridotites at the Vema lithospheric section (Mid-Atlantic Ridge). *Journal of Petrology*, *47*(4), 745–771. https://doi.org/10.1093/petrology/egi092

Cann, J. R., Blackman, D. K., Smith, D. K., McAllister, E., Janssen, B., Mello, S., et al. (1997). Corrugated slip surfaces formed at ridge-transform intersections on the Mid-Atlantic Ridge. *Nature*, *385*(6614), 329–332. https://doi.org/10.1038/385329a0

Cannat, M., Bideau, D., & Hébert, R. (1990). Plastic deformation and magmatic impregnation in serpentinized ultramafic rocks from the Garrett transform fault (East Pacific Rise). *Earth and Planetary Science Letters*, *101*(2–4), 216–232. https://doi.org/10.1016/0012-821x(90)90155-q

Cannat, M., Mevel, C., Maia, M., Deplus, C., Durand, C., Gente, P., et al. (1995). Thin crust, ultramafic exposures, and rugged faulting patterns at the Mid-Atlantic Ridge (22°–24°N). *Geology*, *23*(1), 49–52.

Cipriani, A., Bonatti, E., Brunelli, D., & Ligi, M. (2009). 26 million years of mantle upwelling below a segment of the Mid Atlantic Ridge: The Vema Lithospheric Section revisited. *Earth and Planetary Science Letters*, *285*(1–2), 87–95. https://doi.org/10.1029/2009GC002534

Cipriani, A., Bonatti, E., Seyler, M., Brueckner, H. K., Brunelli, D., Dallai, L., et al. (2009). A 19 to 17 Ma amagmatic extension event at the Mid-Atlantic Ridge: Ultramafic mylonites from the Vema Lithospheric Section. *Geochemistry, Geophysics, Geosystems*, *10*(10). https://doi.org/10.1016/j.epsl.2009.05.046

Dick, H. J. B. (1989). Abyssal peridotites, very slow spreading ridges and ocean ridge magmatism. *Geological Society, London, Special Publications*, *42*(1), 71–105. https://doi.org/10.1144/gsl.sp.1989.042.01.06

Dick, H. J. B., & Bullen, T. (1984). Chromian spinel as a petrogenetic indicator in abyssal and alpine-type peridotites and spatially associated lavas. *Contributions to Mineralogy and Petrology*, *86*(1), 54–76. https://doi.org/10.1007/BF00373711

Dick, H. J. B., Fisher, R. L., & Bryan, W. B. (1984). Mineralogic variability of the uppermost mantle along mid-ocean ridges. *Earth and Planetary Science Letters*, *69*. https://doi.org/10.2973/odp.proc.sr.118.156.1991

Dick, H. J. B., Kvassnes, A. J. S., Robinson, P. T., MacLeod, C. J., & Kinoshita, H. (2019). The Atlantis Bank Gabbro Massif, Southwest Indian Ridge. *Progress in Earth and Planetary Science*, *6*(1), 1–70. https://doi.org/10.1016/0012-821x(84)90076-1

Dick, H. J. B., Lin, J., & Schouten, H. (2003). An ultraslow-spreading class of ocean ridge. *Nature*, *426*, 405–412. https://doi.org/10.1038/nature02128

Dick, H. J. B., Lissenberg, C. J., & Warren, J. M. (2010). Mantle melting, melt transport, and delivery beneath a slow-spreading ridge: The paleo-MAR from 23°15′N to 23°45′N. *Journal of Petrology*, *51*(1–2), 425–467. https://doi.org/10.1093/petrology/egp088

Dick, H. J. B., MacLeod, C. J., Blum, P., Abe, N., Blackman, D. K., Bowles, J. A., et al. (2019). Dynamic accretion beneath a slow-spreading ridge segment: IODP Hole 1473A and the Atlantis Bank Oceanic Core Complex. *Journal of Geophysical Research: Solid Earth*, *124*(12), 12631–12659. https://doi.org/10.1029/2018JB016858

Dick, H. J. B., Natland, J. H., Alt, J. C., Bach, W., Bideau, D., Gee, J. S., et al. (2000). A long in situ section of the lower ocean crust: Results of ODP Leg 176 drilling at the Southwest Indian Ridge. *Earth and Planetary Science Letters*, *179*(1), 31–51. https://doi.org/10.1016/S0012-821X(00)00102-3

Dick, H. J. B., Ozawa, K., Meyer, P. S., Niu, Y., Robinson, P. T., Constantin, M., et al. (2002). Primary silicate mineral chemistry of a 1.5-km section of very slow spreading lower ocean crust: ODP Hole 735B, Southwest Indian Ridge. In *Proceedings of the Ocean Drilling Program, 176 Scientific Results*. Ocean Drilling Program. https://doi.org/10.2973/odp.proc.sr.176.001.2002

Dick, H. J. B., Schouten, H., Meyer, P. S., Gallo, D. G., Bergh, H., Tyce, R., et al. (1991). Tectonic evolution of the Atlantis II fracture zone. In *Proceedings of the Ocean Drilling Program. Scientific Results* (Vol. 118, pp. 359–398). https://doi.org/10.1029/2009gc002534

Dick, H. J. B., Tivey, M. A., & Tucholke, B. E. (2008). Plutonic foundation of a slow-spreading ridge segment: Oceanic core complex at Kane Megamullion, 23°30′N, 45°20′W. *Geochemistry, Geophysics, Geosystems*, *9*(5). https://doi.org/10.1029/2007GC001645

Dien, H., Arai, S., Doucet, L. S., Li, Z. X., Kil, Y., Fougerouse, D., et al. (2019). Cr-spinel records metasomatism not petrogenesis of mantle rocks. *Nature Communications*, *10*(1). https://doi.org/10.1038/s41467-019-13117-1

Elthon, D. (1992). Chemical trends in abyssal peridotites: Refertilization of depleted oceanic mantle. *Journal of Geophysical Research*, *97*, 9015–9025.

Escartín, J., & Canales, J. P. (2011). Detachments in oceanic lithosphere: Deformation, Magmatism, fluid flow, and ecosystems. *Eos, Transactions American Geophysical Union*, *92*(4). 31–31. https://doi.org/10.1029/2011EO040003

Escartín, J., Mével, C., MacLeod, C. J., & McCaig, A. M. (2003). Constraints on deformation conditions and the origin of oceanic detachments: The Mid-Atlantic Ridge core complex at 15°45′N. *Geochemistry, Geophysics, Geosystems*, *4*(8). https://doi.org/10.1029/2002GC000472

Escartín, J., Smith, D. K., Cann, J., Schouten, H., Langmuir, C. H., & Escrig, S. (2008). Central role of detachment faults in accretion of slow-spreading oceanic lithosphere. *Nature*, *455*(7214), 790–794. https://doi.org/10.1038/nature07333

Frost, B. R. (1976). Limits to the assemblage forsterite-anorthite as inferred from peridotite hornfelses, Icicle Creek, Washington. *American Mineralogist*, *61*(7–8), 732–750. https://doi.org/10.1029/92jb00723

Gale, A., Dalton, C. A., Langmuir, C. H., Su, Y., & Schilling, J. G. (2013). The mean composition of ocean ridge basalts. *Geochemistry, Geophysics, Geosystems*, *14*(3), 489–518. https://doi.org/10.1029/2012GC004334

Ghiorso, M. S., Hirschmann, M. M., Reiners, P. W., & Kress, V. C. (2002). The pMELTS: A revision of MELTS for improved calculation of phase relations and major element partitioning related to partial melting of the mantle to 3 GPa. *Geochemistry, Geophysics, Geosystems*, *3*(5), 1–35. https://doi.org/10.1029/2001gc000217

Ghiorso, M. S., & Sack, R. O. (1995). Chemical mass transfer in magmatic processes IV. A revised and internally consistent thermodynamic model for the interpolation and extrapolation of liquid-solid equilibria in magmatic systems at elevated temperatures and pressures. *Contributions to Mineralogy and Petrology*, *119*(2–3), 197–212. https://doi.org/10.1007/BF00307281

Godard, M., Awaji, S., Hansen, H., Hellebrand, E., Brunelli, D., Johnson, K., et al. (2009). Geochemistry of a long in-situ section of intrusive slow-spread oceanic lithosphere: Results from IODP Site U1309 (Atlantis Massif, 30°N Mid-Atlantic-Ridge). *Earth and Planetary Science Letters*, *279*(1–2), 110–122. https://doi.org/10.1016/j.epsl.2008.12.034

Hamlyn, P. R., & Bonatti, E. (1980). Petrology of mantle-derived ultramafics from the Owen Fracture Zone, northwest Indian Ocean: Implications for the nature of the oceanic upper mantle. *Earth and Planetary Science Letters*, *48*(1), 65–79. https://doi.org/10.1016/0012-821X(80)90171-5

Harigane, Y., Michibayashi, K., & Ohara, Y. (2008). Shearing within lower crust during progressive retrogression: Structural analysis of gabbroic rocks from the Godzilla Mullion, an oceanic core complex in the Parece Vela backarc basin. *Tectonophysics*, *457*(3–4), 183–196. https://doi.org/10.1016/0012-821x(80)90171-5

Harigane, Y., Michibayashi, K., & Ohara, Y. (2011a). Deformation and hydrothermal metamorphism of gabbroic rocks within the Godzilla Megamullion, Parece Vela Basin, Philippine Sea. *Lithos*, *124*(3–4), 185–199. https://doi.org/10.1016/j.lithos.2011.02.001

Harigane, Y., Michibayashi, K., & Ohara, Y. (2011b). Relicts of deformed lithospheric mantle within serpentinites and weathered peridotites from the Godzilla Megamullion, Parece Vela Back-Arc Basin, Philippine Sea. *Island Arc*. https://doi.org/10.1111/j.1440-1738.2011.00759.x

Harigane, Y., Okamoto, A., Morishita, T., Snow, J. E., Tamura, A., Yamashita, H., et al. (2019). Melt–fluid infiltration along detachment shear zones in oceanic core complexes: Insights from amphiboles in gabbro mylonites from the Godzilla Megamullion, Parece Vela Basin, the Philippine Sea. *Lithos*, *20*, 174–187. https://doi.org/10.1016/j.lithos.2019.06.019

Hellebrand, E., & Snow, J. E. (2003). Deep melting and sodic metasomatism underneath the highly oblique-spreading Lena Trough (Arctic Ocean). *Earth and Planetary Science Letters*, *216*(3), 2305–2338. https://doi.org/10.1016/S0012-821X(03)00508-9

Hellebrand, E., Snow, J. E., Dick, H. J. B., & Hofmann, A. W. (2001). Coupled major and trace elements as indicators of the extent of melting in mid-ocean-ridge peridotites. *Nature*, *410*(6829), 677–681. https://doi.org/10.1038/35070546

Hellebrand, E., Snow, J. E., Hoppe, P., & Hofmann, A. W. (2002). Garnet-field melting and late-stage refertilization in "residual" abyssal peridotites from the Central Indian Ridge. *Journal of Petrology*, *43*(12), 2305–2338. https://doi.org/10.1093/PETROLOGY/43.12.2305

Hirauchi, K., Segawa, I., Kouketsu, Y., Harigane, Y., Ohara, Y., Snow, J., et al. (2021). Alteration processes recorded by back-arc mantle peridotites from oceanic core complexes, Shikoku Basin, Philippine Sea. *Island Arc*, *30*(1), e12419. https://doi.org/10.1111/IAR.12419

Ildefonse, B., Blackman, D. K., John, B. E., Ohara, Y., Miller, D. J., MacLeod, C. J., et al. (2007). Oceanic core complexes and crustal accretion at slow-spreading ridges. *Geology*, *35*(7), 623–626. https://doi.org/10.1130/G23531A.1

Ishizuka, O., Yuasa, M., Taylor, R. N., & Sakamoto, I. (2009). Two contrasting magmatic types coexist after the cessation of back-arc spreading. *Chemical Geology*, *266*(3–4), 274–296. https://doi.org/10.1016/j.chemgeo.2009.06.014

Johnson, K. T. M., Dick, H. J. B., & Shimizu, N. (1990). Melting in the oceanic upper mantle: An ion microprobe study of diopsides in abyssal peridotites. *Journal of Geophysical Research*, *95*(B3), 2661–2678. https://doi.org/10.1029/JB095iB03p02661

Karig, D. E. (1975). Basin genesis in the Philippine Sea. *Initial Reports of the Deep Sea Drilling Project*, *31*, 857–879.

Karson, J. A. (1990). Seafloor spreading on the Mid-Atlantic Ridge: Implications for the structure of ophiolites and oceanic lithosphere produced in slow-spreading environments. In J. Malpas, E. M. Moores, A. Panayiotou, & C. Xenophontos (Eds.), *Ophiolites and Oceanic Crustal Analogues: Proceedings of the Symposium "Troodos 1987"* (pp. 125–130). Geological Survey Department. https://doi.org/10.2973/dsdp.proc.31.142.1975

Karson, J. A., & Dick, H. J. B. (1983). Tectonics of ridge-transform intersections at the Kane fracture zone. *Marine Geophysical Researches*, *6*(1), 51–98. https://doi.org/10.1007/BF00300398

Kasuga, S., & Ohara, Y. (1997). A new model of back-arc spreading in the Parece Vela Basin, northwest Pacific margin. *The Island Arc*, *6*(3), 316–326. https://doi.org/10.1111/j.1440-1738.1997.tb00181.x

Kelemen, P. B., Kikawa, E., & Miller, D. J., & Expedition 209 Scientist. (2004). *Proceedings of the Ocean Drilling Program. Initial Reports* (Vol. 209). Texas A&M University, Ocean Drilling Program. https://doi.org/10.2973/odp.proc.ir.209.2004

Kelemen, P. B., Shimizu, N., & Salters, V. J. M. (1995). Extraction of mid-ocean-ridge basalt from the upwelling mantle by focused flow of melt in dunite channels. *Nature*, *375*(6534), 747–753. https://doi.org/10.1038/375747a0

Kinzler, R. J., & Grove, T. L. (1992). Primary magmas of mid-ocean ridge basalts 1. Experiments and methods. *Journal of Geophysical Research*, *97*(B5), 6885–6906. https://doi.org/10.1029/91JB02840

Kirby, S. H., & Etheridge, M. A. (1981). Exsolution of Ca-clinopyroxene from orthopyroxene aided by deformation. *Physics and Chemistry of Minerals*, *7*(3), 105–109. https://doi.org/10.1007/BF00308225

Leake, B. E., Woolley, A. R., Arps, C. E. S., Birch, W. D., Gilbert, M. C., Grice, J. D., et al. (1997). Nomenclature of amphiboles: Report of the Subcommittee on Amphiboles of the International Mineralogical Association, Commission on New Minerals and Mineral Names. *American Mineralogist*, *82*(9–10), 1019–1037. https://doi.org/10.1180/minmag.1997.061.405.13

Lian, D., Yang, J., Robinson, P. T., Liu, F., Xiong, F., Zhang, L., et al. (2016). Tectonic evolution of the western Yarlung Zangbo Ophiolitic Belt, Tibet: Implications from the petrology, mineralogy, and geochemistry of the peridotites. *Journal of Geology*, *124*(3), 353–376. https://doi.org/10.1086/685510

Liang, Y., Sun, C., & Yao, L. (2013). A REE-in-two-pyroxene thermometer for mafic and ultramafic rocks. *Geochimica et Cosmochimica Acta*, *102*, 246–260. https://doi.org/10.1016/j.gca.2012.10.035

Loocke, M., Snow, J. E., & Ohara, Y. (2013). Melt stagnation in peridotites from the Godzilla Megamullion Oceanic Core Complex, Parece Vela Basin, Philippine Sea. *Lithos*, *182–183*, 1–10. https://doi.org/10.1016/j.lithos.2013.09.005

Maaløe, S. (1982). Geochemical aspects of permeability controlled partial melting and fractional crystallization. *Geochimica et Cosmochimica Acta*, *46*(1), 43–57. https://doi.org/10.1016/0016-7037(82)90289-7

Macleod, C. J., Banerji, D., Banks, G. J., Irving, D. H. B., Lilly, R. M., Mccaig, A. M., & Smith, D. K. (2002). Direct geological evidence for oceanic detachment faulting: The Mid-Atlantic Ridge, 15°45′N. *Geology*, *30*(10), 879–882. https://doi.org/10.1130/0091-7613(2002)030<0879:DGEFOD>2.0.CO;2

Macleod, C. J., Searle, R. C., Murton, B. J., Casey, J. F., Mallows, C., Unsworth, S. C., et al. (2009). Life cycle of oceanic core complexes. *Earth and Planetary Science Letters*, *287*(3–4), 333–344. https://doi.org/10.1016/j.epsl.2009.08.016

McDonough, W. F., & Sun, S.-S. (1995). The composition of the Earth. *Chemical Geology*, *120*(3–4), 223–253. https://doi.org/10.1016/0009-2541(94)00140-4

Melson, W. G., Jarosewich, E., Bowen, V. T., & Thompson, G. (1967). St. Peter and St. Paul rocks: A high temperature, mantle-derived intrusion. *Science*, *155*, 1532–1535.

Michael, P. J., & Bonatti, E. (1985). Peridotite composition from the North Atlantic: Regional and tectonic variations and implications for partial melting. *Earth and Planetary Science Letters*, *73*(1), 91–104. https://doi.org/10.1126/science.155.3769.1532

Michibayashi, K., Harigane, Y., Ohara, Y., Muto, J., & Okamoto, A. (2014). Rheological properties of the detachment shear zone of an oceanic core complex inferred by plagioclase flow law: Godzilla Megamullion, Parece Vela back-arc basin, Philippine Sea. *Earth and Planetary Science Letters*, *408*, 16–23. https://doi.org/10.1016/j.epsl.2014.10.005

Niu, Y. (1997). Mantle melting and melt extraction processes beneath ocean ridges: Evidence from abyssal peridotites. *Journal of Petrology*, *38*(8), 1047–1329. https://doi.org/10.1093/petroj/38.8.1047

Niu, Y., & Hékinian, R. (1997). Spreading-rate dependence of the extent of mantle melting beneath ocean ridges. *Nature*, *385*(6614), 326–328. https://doi.org/10.1038/385326a0

Ohara, Y. (2016). The Godzilla Megamullion, the largest oceanic core complex on the earth: A historical review. *Island Arc*, *25*(3), 193–208. https://doi.org/10.1111/iar.12116

Ohara, Y., Fujioka, K., Ishii, T., & Yurimoto, H. (2003). Peridotites and gabbros from the Parece Vela backarc basin: Unique tectonic window in an extinct backarc spreading ridge. *Geochemistry, Geophysics, Geosystems*, *4*(7). https://doi.org/10.1029/2002GC000469

Ohara, Y., Kato, Y., Yoshida, T., & Nishimura, A. (2015). Geoscientific characteristics of the seafloor of the Southern Ocean of Japan revealed by Japan's Continental Shelf Survey. *Journal of Geography*, *124*(5), 687–709. https://doi.org/10.5026/jgeography.124.687

Ohara, Y., Okino, K., Akizawa, N., Fujii, M., Harigane, Y., Hirano, N., et al. (2018). A new tectonic window into the backarc basin lower oceanic crust and upper mantle: Mado Megamullion in the Shikoku Basin. *American Geophysical Union, Fall Meeting 2018, abstract #T32C-05B*. Retrieved from https://ui.adsabs.harvard.edu/abs/2018AGUFM.T32C.05O/abstract

Ohara, Y., Okino, K., Akizawa, N., Fujii, M., Harigane, Y., Hirano, N., et al. (2019). Introducing an oceanic core complex in the Shikoku Basin: Mado Megamullion. *Japan Geoscience Union Meeting 2019, SMP30-07*.

Ohara, Y., Okino, K., & Kasahara, J. (2007). Seismic study on oceanic core complexes in the Parece Vela back-arc basin. *Island Arc*, *16*(3), 348–360. https://doi.org/10.1111/j.1440-1738.2007.00591.x

Ohara, Y., Stern, R. J., Ishii, T., Yurimoto, H., & Yamazaki, T. (2002). Peridotites from the Mariana Trough: First look at the mantle beneath an active back-arc basin. *Contributions to Mineralogy and Petrology*, *143*(1), 1–18. https://doi.org/10.1007/s00410-001-0329-2

Ohara, Y., Yoshida, T., Kato, Y., & Kasuga, S. (2001). Giant Megamullion in the Parece Vela Backarc Basin. *Marine Geophysical Researches*, *22*(1), 47–61. https://doi.org/10.1023/A:1004818225642

Okamura, F. P., McCallum, I. S., Stroh, J. M., Ghose, S., Okamura, F. P., McCallum, I. S., et al. (1976). *Pyroxene-spinel intergrowths in lunar and terrestrial pyroxenes* (Vol. 2). LPSC. Retrieved from https://ui.adsabs.harvard.edu/abs/1976LPSC….7.1889O/abstract

Okino, K. (2015). Magnetic anomalies in the Philippine Sea: Implications for regional tectonics. *Journal of Geography*, *124*(5), 729–747. https://doi.org/10.5026/jgeography.124.729

Okino, K., Ohara, Y., Fujii, M., & Hanyu, T. (2019). Evolution of oceanic core complexes in the Shikoku Basin: When backarc basins cease to open. *Japan Geoscience Union Meeting, SCG56-P06*.

Okino, K., Ohara, Y., Kasuga, S., & Kato, Y. (1999). The Philippine Sea: New survey results reveal the structure and the history of the marginal basins. *Geophysical Research Letters*, *26*(15), 2287–2290. https://doi.org/10.1029/1999GL900537

Ozawa, K., & Shimizu, N. (1995). Open-system melting in the upper mantle: Constraints from the Hayachine-Miyamori ophiolite, northeastern Japan. *Journal of Geophysical Research*, *100*(B11), 22315–22335. https://doi.org/10.1029/95jb01967

Pagé, P., Bédard, J. H., Schroetter, J. M., & Tremblay, A. (2008). Mantle petrology and mineralogy of the Thetford Mines Ophiolite Complex. *Lithos*, *100*(1–4), 255–292. https://doi.org/10.1016/j.lithos.2007.06.017

Parnell-Turner, R., Escartín, J., Olive, J. A., Smith, D. K., & Petersen, S. (2018). Genesis of corrugated fault surfaces by strain localization recorded at oceanic detachments. *Earth and Planetary Science Letters*, *498*, 116–128. https://doi.org/10.1016/j.epsl.2018.06.034

Paton, C., Hellstrom, J., Paul, B., Woodhead, J., & Hergt, J. (2011). Iolite: Freeware for the visualisation and processing of mass spectrometric data. *Journal of Analytical Atomic Spectrometry*, *26*(12), 2508–2518. https://doi.org/10.1039/c1ja10172b

Poldervaart, A., & Hess, H. H. (1951). Pyroxenes in the crystallization of basaltic magma. *The Journal of Geology*, *59*(5), 472–489. https://doi.org/10.1086/625891

Rampone, E., Borghini, G., & Basch, V. (2020). Melt migration and melt-rock reaction in the Alpine-Apennine peridotites: Insights on mantle dynamics in extending lithosphere. *Geoscience Frontiers*, *11*(1), 151–166. https://doi.org/10.1016/j.gsf.2018.11.001

Rehfeldt, T., Obst, K., & Johansson, L. (2007). Petrogenesis of ultramafic and mafic xenoliths from Mesozoic basanites in southern Sweden: Constraints from mineral chemistry. *International Journal of Earth Sciences*, *96*(3), 433–450. https://doi.org/10.1007/s00531-006-0116-4

Roux, V. L., Dasgupta, R., & Lee, C. A. (2015). Recommended mineral-melt partition coefficients for FRTEs (Cu), Ga, and Ge during mantle melting. *American Mineralogist*, *100* (11–12), 2533–2544. https://doi.org/10.2138/am-2015-5215

Salters, V. J. M., & Stracke, A. (2004). Composition of the depleted mantle. *Geochemistry, Geophysics, Geosystems*, *5*(5). https://doi.org/10.1029/2003GC000597

Sanfilippo, A., Dick, H. J. B., & Ohara, Y. (2013). Melt-rock reaction in the mantle: Mantle troctolites from the Parece Vela ancient back-arc spreading center. *Journal of Petrology*, *54*(5), 861–885. https://doi.org/10.1093/petrology/egs089

Saumur, B. M., & Hattori, K. (2013). Zoned Cr-spinel and ferritchromite alteration in forearc mantle serpentinites of the Rio San Juan Complex, Dominican Republic. *Mineralogical Magazine*, *77*(1), 117–136. https://doi.org/10.1180/minmag.2013.077.1.11

Sauter, D., Cannat, M., Rouméjon, S., Andreani, M., Birot, D., Bronner, A., et al. (2013). Continuous exhumation of mantle-derived rocks at the Southwest Indian Ridge for 11 million years. *Nature Geoscience*, *6*(4), 314–320. https://doi.org/10.1038/ngeo1771

Sdrolias, M., Roest, W. R., & Müller, R. D. (2004). An expression of Philippine Sea plate rotation: The Parece Vela and Shikoku basins. *Tectonophysics*, *394*(1–2), 69–86. https://doi.org/10.1016/j.tecto.2004.07.061

Seyler, M., Brunelli, D., Toplis, M. J., & Mével, C. (2011). Multiscale chemical heterogeneities beneath the eastern Southwest Indian Ridge (52°E–68°E): Trace element compositions of along-axis dredged peridotites. *Geochemistry, Geophysics, Geosystems*, *12*(9). https://doi.org/10.1029/2011GC003585

Seyler, M., Lorand, J. P., Dick, H. J. B., & Drouin, M. (2007). Pervasive melt percolation reactions in ultra-depleted refractory harzburgites at the Mid-Atlantic Ridge, 15° 20′N: ODP Hole 1274A. *Contributions to Mineralogy and Petrology*, *153*(3), 303–319. https://doi.org/10.1007/s00410-006-0148-6

Seyler, M., Lorand, J. P., Toplis, M. J., & Godard, G. (2004). Asthenospheric metasomatism beneath the mid-ocean ridge: Evidence from depleted abyssal peridotites. *Geology*, *32*(4), 301–304. https://doi.org/10.1130/G20191.1

Shaw, D. M. (1970). Trace element fractionation during anatexis. *Geochimica et Cosmochimica Acta*, *34*(2), 237–243. https://doi.org/10.1029/2011gc003585

Shervais, J. W., Reagan, M., Haugen, E., Almeev, R. R., Pearce, J. A., Prytulak, J., et al. (2019). Magmatic response to subduction initiation: Part 1. Fore-arc basalts of the Izu-Bonin arc from IODP Expedition 352. *Geochemistry, Geophysics, Geosystems*, *20*(1), 314–338. https://doi.org/10.1029/2018GC007731

Smith, D. K., Escartín, J., Schouten, H., & Cann, J. R. (2008). Fault rotation and core complex formation: Significant processes in seafloor formation at slow-spreading mid-ocean ridges (Mid-Atlantic Ridge, 13°–15°N). *Geochemistry, Geophysics, Geosystems*, *9*(3). https://doi.org/10.1029/2007GC001699

Sobolev, A. V., & Shimizu, N. (1992). Ultra-depleted melts and permeability of the oceanic mantle. *Doklady Akademii Nauk*, *236*, 354–360.

Spencer, J. E., & Ohara, Y. (2014). Curved grooves at the Godzilla Megamullion in the Philippine Sea and their tectonic significance. *Tectonics*, *33*(6), 1028–1038. https://doi.org/10.1002/2013TC003515

Stracke, A., Zindler, A., Salters, V. J. M., McKenzie, D., Janne, B. T., Albarède, F., & Grönvold, K. (2003). Theistareykir revisited. *Geochemistry, Geophysics, Geosystems*, *4*(2), 8507. https://doi.org/10.1029/2001GC000201

Sun, C., & Liang, Y. (2012). Distribution of REE between clinopyroxene and basaltic melt along a mantle adiabat: Effects of major element composition, water, and temperature. *Contributions to Mineralogy and Petrology*, *163*(5), 807–823. https://doi.org/10.1007/s00410-011-0700-x

Sun, S.-S., & McDonough, W. F. (1989). Chemical and isotopic systematics of oceanic basalts: Implications for mantle composition and processes. *Geological Society Special Publication*, *42*(1), 313–345. https://doi.org/10.1144/GSL.SP.1989.042.01.19

Taira, A., Ohara, Y., Wallis, S. R., Ishiwatari, A., & Iryu, Y. (2016). Geological evolution of Japan: An overview. In T. Moreno, S. Wallis, T. Kojima, W. Gibbons (Eds.), *The geology of Japan*. (pp. 1–24). Geological Society of London. https://doi.org/10.1144/GOJ.1

Tani, K., Dunkley, D. J., & Ohara, Y. (2011). Termination of backarc spreading: Zircon dating of a giant oceanic core complex. *Geology*, *39*(1), 47–50. https://doi.org/10.1130/G31322.1

Tartarotti, P., Susini, S., Nimis, P., & Ottolini, L. (2002). Melt migration in the upper mantle along the Romanche Fracture Zone (Equatorial Atlantic). *Lithos*, *63*(3–4), 125–149. https://doi.org/10.1016/s0024-4937(02)00116-0

Taylor, W. (1998). An experimental test of some geothermometer and geobarometer formulations for upper mantle peridotites with application to the thermobarometry of fertile lherzolite and garnet websterite. *Neues Jahrbuch für Mineralogie - Abhandlungen*, *172*, 381–408. https://doi.org/10.1016/s0024-4937(02)00116-0

Tucholke, B. E., Behn, M. D., Buck, W. R., & Lin, J. (2008). Role of melt supply in oceanic detachment faulting and formation of megamullions. *Geology*, *36*(6), 455–458. https://doi.org/10.1130/G24639A.1

Tucholke, B. E., Lin, J., & Kleinrock, M. C. (1998). Megamullions and mullion structure defining oceanic metamorphic core complexes on the Mid-Atlantic Ridge. *Journal of Geophysical Research: Solid Earth*, *103*(5), 9857–9866. https://doi.org/10.1127/njma/172/1998/381

Wang, C., Liang, Y., & Xu, W. (2021). Formation of amphibole-bearing peridotite and amphibole-bearing pyroxenite through hydrous melt-peridotite reaction and in situ crystallization: An experimental study. *Journal of Geophysical Research: Solid Earth*, *126*(3), e2020JB019382. https://doi.org/10.1029/2020JB019382

Warren, J. M., & Shimizu, N. (2010). Cryptic variations in abyssal peridotite compositions: Evidence for shallow-level melt infiltration in the oceanic lithosphere. *Journal of Petrology*, *51*(1–2), 395–423. https://doi.org/10.1093/petrology/egp096

Workman, R. K., & Hart, S. R. (2005). Major and trace element composition of the depleted MORB mantle (DMM). *Earth and Planetary Science Letters*, *231*(1–2), 53–72. https://doi.org/10.1016/j.epsl.2004.12.005

Xiong, F., Dilek, Y., Wirth, R., Xu, X., & Yang, J. (2020). Opx–Cpx exsolution textures in lherzolites of the Cretaceous Purang Ophiolite (S. Tibet, China), and the deep mantle origin of Neotethyan abyssal peridotites. *International Geology Review*, *62*(6), 665–682. https://doi.org/10.1080/00206814.2019.1627678

Zhang, W.-Q., Liu, C.-Z., & Dick, H. J. B. (2021). Evidence for Multi-stage Melt Transport in the Lower Ocean Crust: The Atlantis Bank Gabbroic Massif (IODP Hole U1473A, SW Indian Ridge). *Journal of Petrology*, *61*(9). https://doi.org/10.1093/petrology/egaa082

Zhu, Y., Chen, J., Xue, Y., Feng, W., & Jiang, J. (2018). Spinel and orthopyroxene exsolved from clinopyroxene in the Haladala pluton in the middle Tianshan (Xinjiang, China). *Mineralogy and Petrology*, *112*(4), 465–479. https://doi.org/10.1007/s00710-017-0549-4